ACS OMEGA

Open Access

http://pubs.acs.org/journal/acsodf

Review

Colloidal Quantum Dots as an Emerging Vast Platform and Versatile Sensitizer for Singlet Molecular Oxygen Generation

Zahid U. Khan,* Latif U. Khan, Hermi F. Brito, Magnus Gidlund, Oscar L. Malta, and Paolo Di Mascio*

Cite This: *ACS Omega* 2023, 8, 34328−34353

Read Online

ACCESS | Metrics & More | Article Recommendations

ABSTRACT: Singlet molecular oxygen ($^1O_2$) has been reported in wide arrays of applications ranging from optoelectronic to photooxygenation reactions and therapy in biomedical proposals. It is also considered a major determinant of photodynamic therapy (PDT) efficacy. Since the direct excitation from the triplet ground state ($^3O_2$) of oxygen to the singlet excited state $^1O_2$ is spin forbidden; therefore, a rational design and development of heterogeneous sensitizers is remarkably important for the efficient production of $^1O_2$. For this purpose, quantum dots (QDs) have emerged as versatile candidates either by acting individually as sensitizers for $^1O_2$ generation or by working in conjunction with other inorganic materials or organic sensitizers by providing them a vast platform. Thus, conjoining the photophysical properties of QDs with other materials, e.g., coupling/combining with other inorganic materials, doping with the transition metal ions or lanthanide ions, and conjugation with a molecular sensitizer provide the opportunity to achieve high-efficiency quantum yields of $^1O_2$ which is not possible with either component separately. Hence, the current review has been focused on the recent advances made in the semiconductor QDs, perovskite QDs, and transition metal dichalcogenide QD-sensitized $^1O_2$ generation in the context of ongoing and previously published research work (over the past eight years, from 2015 to 2023).

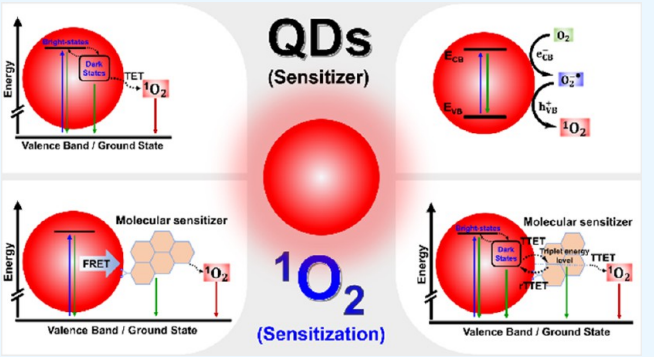

1. INTRODUCTION

Singlet molecular oxygen [$^1O_2$ ($^1\Delta_g$)], interchangeably written as $^1O_2$, is the lowest excited state oxygen of the triplet molecular oxygen ground state [$^3O_2$ ($^3\Sigma_g^-$)], which is a potent electrophilic, highly reactive, and short-lived species.[1−8] The activation of triplet molecular oxygen was initially reported by Kautsky in 1938 while working with the photo-oxidation of fluorescence dyes where activated oxygen was produced.[9] In 1960, Seliger detected the generation of activated oxygen in the form of faint red light emitted from a mixture of sodium hypochlorite and hydrogen peroxide with a low-resolution photomultiplier.[10] The faint red light was later validated by Khan and Kasha in 1963 by photographing chemiluminescence, and they termed it an excited state of molecular oxygen.[11] In 1964, Foote and Wexler confirmed the formation of activated oxygen in photosensitized reactions.[12] Thus, since its discovery, $^1O_2$ has provoked a great deal of interest in the scientific community, using in a wide array of applications such as cancer therapeutics,[6−8,13,14] antiparasitic and antimicrobial,[2,4,15−18] stereoselective photochemical synthesis,[19] oxidation of organic pollutants in wastewater treatment,[2,7] and photochemical upconversion.[20] Principally, $^3O_2$ is inert to biomolecules because the two unpaired electrons with parallel spins are located in two separate π^* molecular orbitals, which give it low redox potential (−0.16 V). The strong oxidizing property of $^1O_2$ arises from electron pairing in one of these two degenerate π^* molecular orbitals, while the other π^* orbital remains unoccupied.[4,7] Thus, the presence of an empty π^* orbital imparts strong acidic properties (i.e., accepting an electron pair) to $^1O_2$.[7,21] Singlet molecular oxygen plays multiple key roles in the physiological processes of living organisms: it is involved in sterilizing immunity (such as a defensive tool in phagocytes against bacteria and viruses);[4,22] it is associated with triggering ultraviolet A (UV-A)-induced biological effects through activation of gene expression and oxidative genotoxicity and is involved in the lipoperoxidation process;[23−25] it acts as a messenger in cell signaling;[26] and it is involved in the alteration of the permeability of epithelial mitochondrial membranes and the metabolism of many living organisms.[3,4] In biological systems, $^1O_2$ may be produced by two processes: light-dependent and light-independent (dark reactions).[27] During the dark reactions, $^1O_2$ can be produced by oxygenases (lipoxygenases)[28] or peroxydases (myeloperoxidase),[29] the

Received: June 7, 2023
Accepted: August 15, 2023
Published: September 11, 2023

reaction of ozone with biomolecules,[30,31] the reaction of hydrogen peroxide (H_2O_2) with hypochlorite (ClO^-) or peroxynitrite,[32−34] and the thermodecomposition of dioxetanes.[35,36] However, the light-dependent process involves endogenous photosensitizers, which upon excitation by the UV component of solar radiations transfer energy from the triplet excited state to ground state oxygen by type II photosensitization.[4,37] Beside, several chemical sources can convert $^3O_2$, in the dark, into $^1O_2$ with quantitative yields. Some of them include the disproportionation of H_2O_2 by MoO_4^{2-}, oxidation of ClO^- by H_2O_2, base-catalyzed disproportionation of peracids, and the reduction of ozone by triphenyl phosphite.[4,38,39] Unfortunately, the translation of these reactions into biological systems is not possible due to the noncompatibility with the physiological environment.[4]

Since the direct excitation from the triplet ground state of oxygen to the singlet excited state is spin forbidden, different extended conjugated π-electronic systems containing organic or metalorganic photosensitizers (PS) are used to generate $^1O_2$ by transferring energy from the excited triplet state of PS to $^3O_2$, which in turn converts the $^3O_2$ into $^1O_2$ and leaves the PS at its ground state.[1,4,6−8,13] However, the sensitizers based on conjugated π-electronic systems have significant disadvantages such as insolubility in aqueous media, poor photochemical stability, poor target selectivity, low extinction coefficients, a narrow absorption band, and large singlet−triplet splitting (hundreds of meV).[5,13,40,41] Therefore, for efficient and persistent $^1O_2$ generation, PS of high performance having a high oxidation tolerance are strongly required.[7] One way of addressing these problems is through nanoscale architecture, such as the incorporation of PS into dendrimeric or polymeric materials, encapsulation in liposomes, or inclusion of PS in hybrid core−shell nanoparticles (NPs) or porous nanomaterials (NMs).[1,5,8,42] The nanoformulation of PS along with other multifunctionalities provides additional potential diagnostic information, imaging-guided highly precise delivery to a site of interest, accurate localization, and therapeutic benefits at the same time.[8,42,43] For this purpose, QDs have emerged as high performance and versatile nanotools due to their unique physicochemical and size-dependent optoelectronic properties.[5] Besides, the optoelectronic properties of QDs can be manipulated by other parameter such as by fine-tuning their composition via gradient alloying[44,45] or ion exchange (cationic/anionic) induced alloying[46−50] or by the mutual alignment of the valence band (VB) and conduction band (CB) of core and shell materials in core−shell heterostructures,[51−54] which make them superior to the other photoluminescence materials.

Semiconductor QDs have been shown to be highly efficient sensitizers for $^1O_2$ production either individually or functionalized with other inorganic materials or molecular sensitizers.[20,43,55−60] Individually, QDs can be light activated to produce $^1O_2$ via triplet energy transfer (TET)[5,61−65] or charge transfer[21,63,66,67] or energy transfer from dopant defects[68] to dioxygen. On the other hand, QDs functionalized with molecular acceptors involve QDs energy transfer to a molecular acceptor which subsequently sensitizes $^1O_2$ production.[43,55−60,69−71] Thus, QDs offers distinct advantages over the conventional molecular and inorganic nanosensitizers (i.e., polymeric NPs, plasmonic NPs, metallic NPs, lanthanide NPs, etc.) in terms of versatile sensitization of $^1O_2$ generation by various mechanisms and fine-tuning of their optoelectronic properties by multiple parameters in the wide UV−vis and NIR-I (700−900 nm) and NIR-II (1000−1700 nm) regions.[5,14,20,51,54,64,65,72,73]

This review focuses on the recent developments in the QD-assisted emerging strategies for enhanced photosensitized $^1O_2$ generation via different mechanisms: (i) direct energy transfer from the dark states/triplet states of QDs to ground-state oxygen producing $^1O_2$,[5,61−65] (ii) charge transfer from the QDs conduction band (CB) to dioxygen forming $O_2^{-\bullet}$ which subsequently interacts with the valence band (VB) to produce $^1O_2$,[21,63,66,67] and (iii) QD−PS conjugates involving the QDs energy transfer to the PS via Förster resonance energy transfer (FRET),[43,55−57,69−71] Dexter-like energy transfer (DET), or sequential triplet−triplet energy transfer (TTET),[58−60] which subsequently sensitize $^1O_2$ generation.[20,43,55−60]

1.1. Biomedical Applications of Singlet Molecular Oxygen.

1.1.1. Photodynamic Therapy. Owing to its strong oxidizing nature, $^1O_2$ exhibits high reactivity toward electron-rich organic substrates such as olefins, dienes, and polycyclic aromatic compounds.[4,38] It is shown as one of the major cytotoxic species implicated in photodynamic therapy (PDT) of cancerous tissues[5−7,13,14,17,42,53,74,75] and diseases such as porphyria[74] and cataracts.[76] Singlet oxygen is aslo used as an effective tool to inactivate or kill the pathogens, i.e., bacteria, viruses, and fungi.[15,64,77] It reacts readily with electron-rich/unsaturated substrates such as DNA, RNA, unsaturated fatty acids, and cholesterol and protein/amino acids such as cysteine, histidine, methionine, tryptophan, and tyrosine methionine, forming endoperoxides, hydroperoxides, and dioxetanes.[2,4−6,8,31,53,78−80] Thus, the damage induced to biomolecules leads to a cascade of reactions culminating in several biological events: (1) necrosis/or apoptosis of tumor cells; (2) destruction of tumor microvasculature and platelet aggregation; and (3) stimulation of autoimmune and inflammatory responses that eliminate the remaining tumor cells.[8,53]

1.1.2. Smart Drug Delivery. The nanoformulation of smart drug delivery has opened a new avenue in clinical practices to achieve a highly precise and on-demand controlled release of therapeutic agents[81] at a specific location, thus improving the treatment efficacy while minimizing/evading the off-site problems. In the system, the therapeutic agents are conjugated/chemically linked with a light-sensitive photosensitizer. Upon exposure to light, the photosensitizers produce $^1O_2$ which triggers the release of therapeutic agents at a site of interest and a desired time.[81−84] For example, Mo et al.[83] developed singlet oxygen-responsive light-activated siRNA endosomal release (LASER) using porphyrin lipid nanoparticle (LNP) encapsulated siRNA to achieve an enhanced siRNA endosomal escape and significantly improved knockdown efficacy. The porphyrin lipids enabled LNPs to generate $^1O_2$ upon light irradiation which disrupted the endosomal membrane, therby triggering siRNA endosomal escape to cytosol.[83]

1.1.3. Biomaterial Modifications. Singlet oxygen is often employed in biomaterial sciences to modify the functionalities or enhance the biocompatibility of biomolecules or therapeutic agents/medical devices. For example, it can be utilized in peptide and protien modification,[84−86] i.e., proteins−protein cross-linking and protein knockdown, conjugating fluorescence tags to biomolecules, and protein/enzyme immobilization on material surfaces for biocatalysis and biosensing,[85,86] etc. Singlet oxygen-responsive protein−protein cross-linking plays a vital role in various biochemical processes including environmental sensing, signal transduction, and maintaining cellular organ-

https://doi.org/10.1021/acsomega.3c03962
ACS Omega 2023, 8, 34328−34353

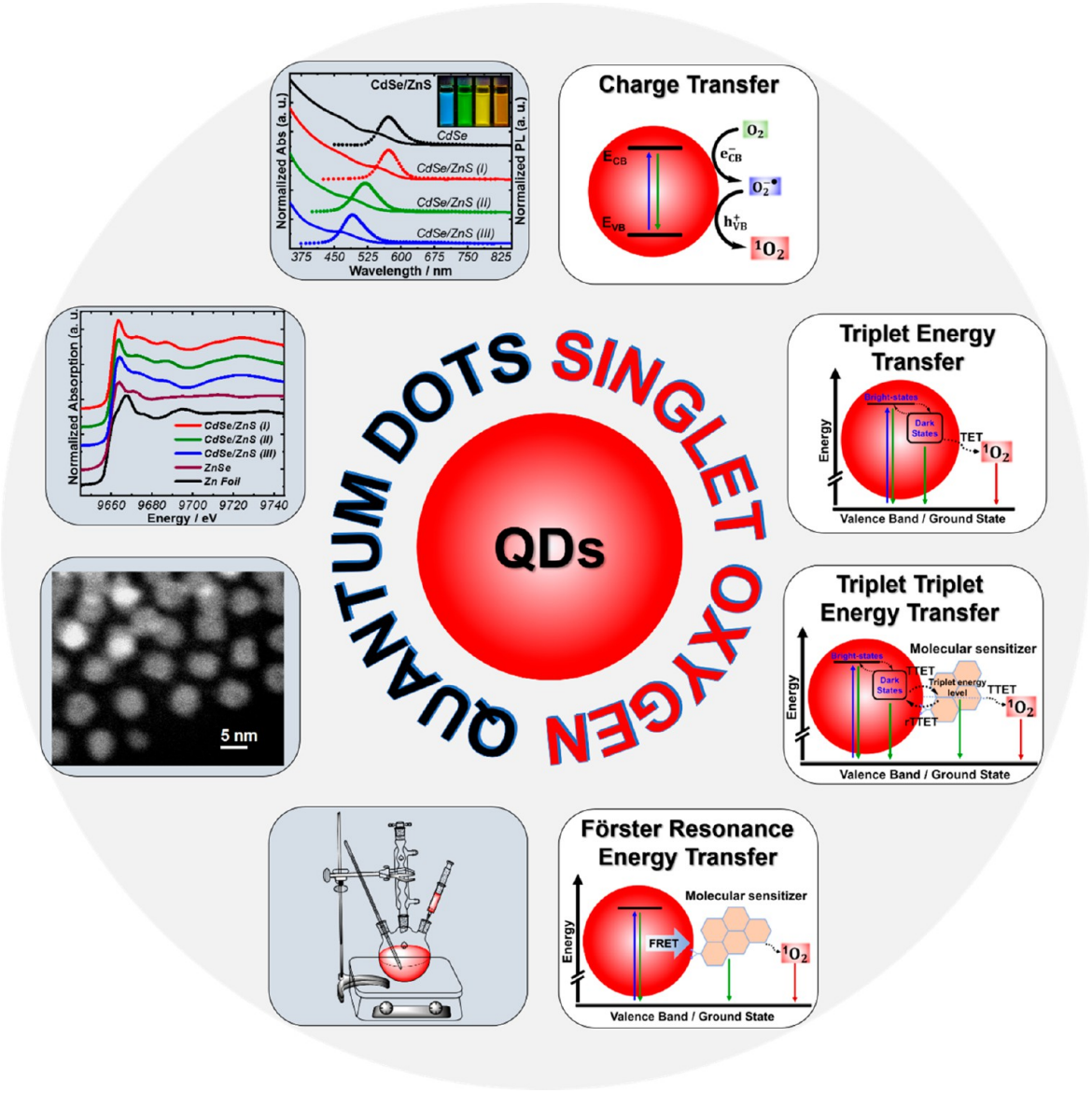

Figure 1. Schematic illustration of the synthesis and complementary characterization techniques for QDs with possible sensitization pathways for singlet molecular oxygen ($^1O_2$) generation.

ization. For example, singlet oxygen-responsive protein−protein cross-linking is used for for wound suturing, tissue repair, tissue bioprinting where photoactivated materials derive the formation or degradation of chemical bonds with spatiotemporal control,[87] and treatment of accommodative intraocular lenses to reverse presbyopia.[84,86,88]

2. FUNDAMENTAL OPTOELECTRONIC PROPERTIES OF QDS

Quantum dots (QDs) are a new type of ultrasmall condensed matter particles that have drawn highly fundamental and applied interest as potential vehicles for photodynamic therapy. Their characteristic optoelectronic properties, owing to the quantum confinement in individual QDs, leading to novel exciton generation and recombination in the intrabandgap, provided remarkably relevant energy/electron transfer features for optical applications.[42,54,89,90] For instance, QDs are potential sensitizers, individually[5,21,61−67] or together with organic photosensitizers[43,55−60,69−71] as surface carriers for singlet molecular oxygen ($^1O_2$) generation. The mechanistic approach toward the sensitization of singlet oxygen generation by QDs, involving energy transfer and migration between the sensitizer and molecular oxygen, is a challenging task. The reported studies have revealed that it usually occurs through the triplet energy transfer pathway.[5] Thus, detailed optical properties along with an insight into the electronic structure are paramount to probe the sensitization mechanism of the singlet oxygen generation.

X-ray absorption spectroscopy (XAS) is a highly element-specific technique that probes efficiently the local atomic/electronic structure of the photoabsorber (metal site) in NCs.[91] The lattice disorder, oxygen vacancies, and defects in the lattice can be probed by quantitative X-ray absorption near-edge spectroscopy (XANES) and extended X-ray absorption fine structure (EXAFS) analyses.[5,90] The emission color of the QDs is extended over the wide visible to near-infrared (NIR) wavelength ranges, mainly due to the size-dependent quantum confinement effects, originating from the spatial confinement of electron−hole pairs (excitons) in one or more dimensions

https://doi.org/10.1021/acsomega.3c03962
ACS Omega 2023, 8, 34328−34353

within a material, carrying a discrete electronic energy level structure when compared to the bulk material counterparts.[5,20,42,53,75,89,90,92] The quantum confinement effect usually occurs in semiconductors, when the particle sizes are reduced to the same order as the exciton radius, i.e., to a few nanometers, providing modified exciton properties with a changeable bandgap in relation to the size of the nanocrystal. Usually, reported studies have revealed that the emission wavelengths of QDs have been tuned by either changing their size and shape or doping with d-transition metals/lanthanide ions.[89,90] Nevertheless, Khan and co-workers[5] have recently reported the tuning of the emission colors from orange to blue based on interfacial ion exchange (predominantly exchange of Se^{2-} by the S^{2-} anion) for the CdSe/ZnS core/shell nanocrystals with a similar crystal size. They probed the interfacial anion exchange in core/shell lattices of the QDs by quantitative extended X-ray absorption spectroscopy (EXAFS) data analyses and demonstrated that the increase in the exchange of selenide by a sulfide anion in the core lattice caused blue shifting in emission band regions from the orange to blue. Thus, it is worthwhile to mention that an integrated approach of complementary characterization techniques, for instance, studying size-dependent morphological behavior of QDs by transmission electron microscopy, electronic/local atomic structure of their lattice by XAS together with probing emission by optical spectroscopy, and $^1O_2$ detection, is required to gain detail knowledge on the sensitization of singlet oxygen ($^1O_2$) generation by quantum dots (Figure 1).

Hence, this review focuses on the recent designs and advancement of $^1O_2$ sensitizers based on three different types of quantum dots: (i) semiconductor quantum dots, (ii) perovskite quantum dots, and (iii) transition metal dichalcogenide quantum dots. Therefore, in this section, we discuss the optoelectronic properties of the above-mentioned QDs by using different spectroscopic techniques.

2.1. Semiconductor QDs. Recently, inorganic photochemistry has emerged as highly performant and versatile for potential use in $^1O_2$ generation for photodynamic therapy.[5,43,59,64,67] For this purpose, semiconductor QDs represent one of the leading quantum materials in the inorganic chemistry area. Quantum dots are tiny light-emitting particles (1−10 nm)[51,53,75] made up of hundreds to thousands of atoms, such as I and VI (e.g., Ag_2X, X: S, Se, and Te),[14,42,54] II and VI (ZnX and CdX, X: S, Se, and Te),[14,20,41,42,51,53,54,89,90,93] III and V (InAs, InP, InSb, GaAs, and GaSb),[14,42,51,59] IV and VI (PdX, X: S, Se, and Te),[20,41,42,51,94] and I, III and VI_2 groups ($AgInX_2$, $CuInX_2$, X: S, Se, and Te).[42,51,54,64,73,92]

It is noteworthy that the semiconductor QDs were initially reported in the early 1980s by Ekimov[42,95] and Brus[96] as nanoscale-size crystals in the glassy matrix and colloidal solutions, respectively. After more than 30 years since their discovery, the growing progress in QD materials has led to their use in a vast array of applications such as biolabeling, biosensing, multiplexed bioimaging, selective targeting, diagnostics, and nanotheranostics.[5,14,42,54,73,75,89,90,92,93] QDs are considered an intermediate species between atoms or molecules as well as bulk materials, which combine the different features that are found individually either only in bulk inorganic materials or in organic molecules.[42,54] The key characteristics of the QDs are the bandgap widening, discretization of electronic states, and quantum confinement effect when the particle size dwindles to a length scale lesser than Bohr's radii.[5,20,42,53,75,92] The photoluminescence properties of QDs originate from the radiative recombination of photogenerated charged carriers (electron−hole pair) due to the quantum confinement effect.[42,54,89,90] Under light exposure, an electron−hole pair (also known as an *exciton*) (Figure 2a) is generated by exciting

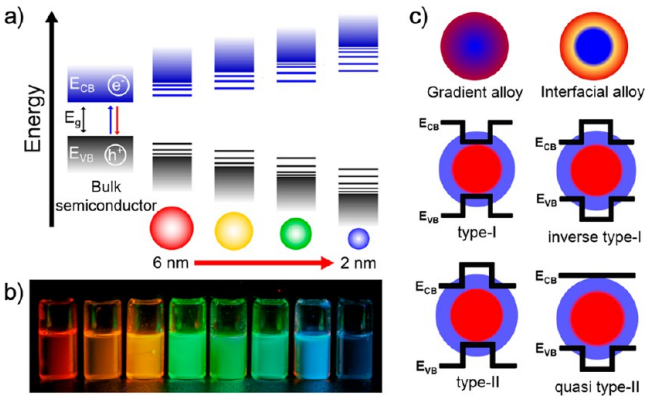

Figure 2. Representation of the photogenerated electron−hole pair (exciton), radiative recombination of the exciton, the NC size effect on quantum confinement, and the respective emission color of QDs (a). Photographs of luminescent CdSe/ZnS QDs under UV light irradiation (b). Gradient alloy, interfacial alloy (right top row), and representative diagrams of bands alignment (right middle to bottom row) in core−shell quantum dots (c).

the electron to the quantized band structure depending upon the transition probabilities. Subsequently, the exciton is relaxed back, releasing the energy through various pathways: phonon-assisted relaxation, exciton radiative recombination, non-radiative decay due to surface states/traps, auger recombination, electronic energy transfer to the vibrational energy level of ligands, etc.[42,51,53,73,75]

The optoelectronic properties of QDs originate from size-dependent quantum confinement effects; therefore, changing the size and shape of the PL emission can be predictably tuned over a wide wavelength range (Figure 2a,b), such as from the UV−vis to NIR-I (700−900 nm) and NIR-II (1000−1700 nm) regions.[14,20,64,65,72,73] Additionally, QDs also present upconversion optical features by converting multiple low-energy photons into a single high-energy photon.[52,65] Thus, due to their unique spectroscopic properties, QDs have excelled as traditional organic dyes, having 100−200 times better photochemical stability, 10−50 times larger extinction coefficients, longer lifetime than those of luminescent dyes, comparatively narrower emission bands, and 10−20 times brighter luminescence.[42,72,75] Recent advances have led to the development of emission color-tunable QDs without changing their size by manipulating their composition effect (Figure 2c) via gradient alloying[51,70,73,92] or cationic (metal) and anionic (chalcogenides) induced interfacial alloying/exchange[5] or judicious incorporation of dopant impurities, i.e., d transition metals and lanthanide ions.[14,42,51,54,63,64,89,90] These additional features provide a new platform to engineer QDs of similar size with different desired photonic properties.

Furthermore, the optoelectronic properties can also be modulated by the mutual alignment of the valence band (VB) and conduction band (CB) of core and shell materials in core−shell heterostructures (Figure 2c). Hence, by tailoring the shell thickness, the optoelectronic properties can be designed and tuned, which is usually unachievable with discrete QDs of either core or shell materials.[51,52] Based on the alignment of the CB

https://doi.org/10.1021/acsomega.3c03962
ACS Omega 2023, 8, 34328−34353

and VB in core−shell heterostructures, QDs have been classified into different types: type-I, inverse type-I, type-II, and quasi-type-II heterostructures.[51,53,54] In type-I materials, the bandgap of the core is smaller and is sandwiched within shell materials of the wider bandgap (Figure 2c). As a result, both charged carriers are completely cordoned off in the core by the shell, and the bandgap emission is almost preserved or undergoes a small red shift.[5,43,51,90,97] Contrarily, in the inverse type-I QDs, the bandgap of the shell is localized in the bandgap of the core, and the electron−hole pair is confined entirely or partially in the shell. Upon increasing the shell thickness, the heterostructure QDs, bandgap alignment is switched from type-I to type-II or quasi-type-II structure, where the VB or CB of the shell material lies within the bandgap of the core (type-II), or the band alignment is flat and the offset between conduction band edge states of the core and shell smaller (quasi type-II).[51] Thus, the exciton is spatially segregated over the entire QDs (Figure 2c). In type-II QDs the charge carrier recombination occurs across the core−shell interface, and consequently, the PL emission wavelength is smaller than that of the bandgap comprising materials due to spatially indirect transitions.[54] It is noteworthy that in the core−shell heterostructure the lattice mismatch between the two crystalline materials with different lattice parameters is a crucial factor to be considered during shell growth. A larger mismatch causes the stress at the interface, which is relieved by generating interfacial misfit dislocations that act as nonradiative centers and reduce the quantum yield (QY).[5,54]

Relatively large spin−orbit coupling is another remarkable property of QDs, which in conjunction with the crystal field causes fine splitting of the excitonic states into close energy spacing (1−15 meV) between the bright and dark states.[20,98,99] The exchange interaction in QDs between the $S = \pm 1/2$ electron and $J = \pm 3/2$ hole produces excitons with total angular momenta projections $|N_m| = 1$ and 2. Since the spin angular momentum of a single photon is 1, the optical transition of $|N_m| = 1$ is dipole allowed (known as a bright exciton, BE), whereas $|N_m| = 2$ is dipole forbidden (known as a dark exciton, DE).[41,100] Therefore, the BEs having antiparallel spins assume singlet-like character, while the parallel spins of the DE give it a triplet-like character.[41,100] These triplet excited states of QDs are remarkably important in the photochemistry area because of their exceptionally long lifetime enabled by the spin-forbidden nature of their recombination, which provides them a long enough time window for many chemical transformations, such as photoredox catalysis, photocycloaddition, and photoisomerization. Additionally, the spin configuration of triplet states allows access to unique chemical reactivity with $^3O_2$ via TET to produce $^1O_2$; thus, the QDs act like molecular sensitizers.[41]

2.2. Perovskite QDs. Perovskite quantum dots are another unprecedented class of semiconductors with a broad range of optoelectronic properties represented with the general chemical formula ABX_3, where A is a monovalent alkali (Cs^+ and Rb^+) and methylammonium cation ($CH_3NH_3^+$ and $CH(NH)_2^+$); B is a bivalent cation (Ge^{2+}, Pb^{2+}, and Sn^{2+}); and X is a monovalent anion (Cl^-, Br^-, and I^-).[40,61,62,66,68] These kind of QDs possess outstanding intrinsic features of direct bandgaps, strong light−matter interactions, broadband absorption, large light-absorption coefficients, reduced PL blinking, high electron−hole mobility, and long carrier diffusion length and are spectrally tunable from ultraviolet to NIR by changing the proportions or replacing the A-site monovalent cation or X-site halogen anion.[40,62,68] Perovskite QDs are highly tolerant to dopant impurities which impart them additional new optical, magnetic, and electronic properties.[68] The other advantage is that they are not difficult to prepare and are compatible with room-temperature deposition processes. Owing to these unique properties, perovskite QDs hold great promise for photovoltaics, lasers, color-tunable light-emitting diodes (LEDs), photodetectors, and phototransistor applications.[68]

2.3. Transition Metal Dichalcogenide QDs. Two-dimensional transition metal dichalcogenide (TMD) QDs with a comparable structure to graphene have attracted growing interest during the past years in the energy, environment, and nanomedicine fields.[101] Among them, the TMDs with stoichiometric combinations (MX_2) of transition metals (M: Mo, W, Ni, Ru, etc.) and chalcogens (X: S, Se, and Te) possess strong in-plane bonding and weak out-of-plane interactions which give them unique X−M−X sandwich structures.[17,102−106] The optoelectronic properties of TMDs are widely tunable by the combined mechanisms of quantum confinement, doping, strain, external fields, and environmental effects. Atomic defects originating from vacancies give them additional unique optical, chemical, physical, and electrical properties.[102,105] Owing to the layered structure, TMD has a large surface area and an increased number of potential binding sites for different molecules.[106] Therefore, these unique features make them attractive materials for transistors, photodetectors, organic light-emitting diodes, solar cells, catalysis, gas sensors, diagnosis, and therapy.[18,101]

3. PHOTOPHYSICS OF SINGLET MOLECULAR OXYGEN

3.1. Fundamentals of $^1O_2$ Generation. Molecular oxygen in the ground electronic state has two parallel spins for two unpaired electrons in its outer orbital, labeled as a triplet state or $O_2(^3\Sigma_g^-)$, while its two higher-energy excited state species, $O_2(^{13}\bigtriangledown_g^+)$ and $O_2(^1\Sigma_g^+)$, consist of the antiparallel electron, resembling singlet electronic states.[4] The $O_2(^1\bigtriangledown_g^+)$ lies 22 kcal above triplet oxygen, whereas $O_2(^1\Sigma_g^+)$ has an energy of 37 kcal above that of the ground state.[4] Due to the extremely short-lived (<1 ns)[7] and fast deactivation of the latter, only the first excited singlet state $O_2(^1\bigtriangledown_g^+)$ will be considered in this review . The singlet oxygen in the excited state relaxes back to the triplet states $[O_2(^1\bigtriangledown_g^+) \rightarrow O_2(^3\Sigma_g^-)]$ and $[O_2(^1\Sigma_g^+) \rightarrow O_2(^3\Sigma_g^-)]$, emitting the extra energy in the form of phosphorescence at around 1270 and 762 nm, respectively.[7,58,71] The direct excitation from the triplet ground state of oxygen ($^3O_2$) to the singlet excited state ($^1O_2$) is spin forbidden (spin-flip process); therefore, the photosensitizers (PS) are necessary to generate $^1O_2$ by transferring energy from the excited triplet state of the PS to the ground state of $^3O_2$[4−8,13,53,75] (Figure 3). Photosensitizers in the excited state undergo intersystem crossing (ISC), populating a long-lived, lower energy triplet excited state (T_1). The electron in the triplet state either returns to the ground state, emitting the energy via phosphorescence, or interacts with other molecules to promote reactive species through two different reactions: (i) In the type I process, the activated PS interacts with biological substrates to form free radicals such as anions or cations by transferring electrons or abstraction of the proton. The generated ROS such as superoxide ($O_2^{-\bullet}$) may undergo further oxidation/reduction, producing hydroxyl radicals ($HO^\bullet$) and hydrogen peroxide (H_2O_2). (ii) In the type II process,[25,37,107] the excited triplet state interacts directly with $^3O_2$ producing $^1O_2$[4−8,53,75] (Figure 3). It is noteworthy that reaction types I and II proceed simultaneously in a competitive

https://doi.org/10.1021/acsomega.3c03962
ACS Omega 2023, 8, 34328−34353

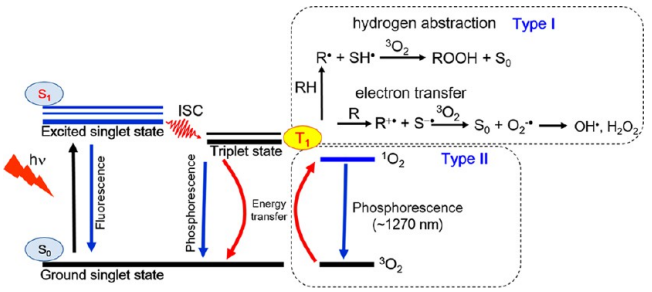

Figure 3. Schematic illustration of photosensitizer (PS) activation, energy transfer via ISC, triplet−triplet energy transfers between the PS and $^3O_2$, and the formation of $^1O_2$ (type I) and ROS (type II). (S: sensitizer; S_0: ground singlet state; S_1: excited singlet state; ISC: intersystem crossing; T_1: triplet excited state).

manner;[108] however, the ratio of both depends upon the type of sensitizers, the concentration of molecular oxygen, and the substrate category. In clinical practices, the efficiency of $^1O_2$ generation by a type II reaction is considered to be the principal determinant of PDT efficacy.

3.2. Detection of $^1O_2$. To date, different methods have been developed to detect singlet oxygen $^1O_2$: (i) directly, by recording the photophysical radiative properties of $^1O_2$, i.e., from the phosphorescence emission at 1270 nm or phosphorescence decay curves by monitoring the emission at 1270 nm,[5,58−60,109] or by recording EPR spectra in the gas phase owing to the paramagnetic properties of $^1O_2$ and (ii) indirectly, by using some standard chemical reporter/probe which reacts with $^1O_2$, producing chemically isolatable or spectroscopically detectable products or intermediates[5,7,61,110] (Figure 4). Thus, the products or intermediate species produced are subsequently identified by chemiluminescence (CL), EPR, absorption, and fluorescence spectroscopy techniques, for each of which some of the commercially available probes include fluoresceinylcypridina luciferin analogues (FCLA), 2,2,6,6-tetramethylpiperidine (TEMP), 1,3-diphenylisobenzofuran (DPBF), and singlet oxygen sensor green (SOSG), respectively.[7,111]

3.3. Limitations of Molecular Sensitizers. Enhancing $^1O_2$ generation is an important strategy to achieve maximum therapeutic efficacy in the PDT treatment of tumors and cancer. Traditional PDT is usually performed by using various organic or metalloorganic sensitizers.[6,8,13] However, despite their success and advancement, conventional molecular sensitizers are subject to multiple significant intrinsic limitations: (1) most of the PS have hydrophobic extended π networks, thus rendering them poor aqueous solubility and aggregation in aqueous solution;[6,53] (2) they have poor photostability and are prone to photodegradation at irradiation for prolonged time, releasing phototoxic products;[13,14] (3) they have characteristically large singlet−triplet splitting (hundreds of meV),[19,41] thus the indirect access to the triplet excited state of a molecular photosensitizer is energy consuming (over 300 eV energy losses can occur)[5,112] and requires high energy UV illumination which may lead to PS photobleaching and photodegradation;[6] (4) they show narrow absorption bands and are excited by UV−visible light which has less penetration capability, thus making them less successful for deep rooted and bulky tumors;[6,8,14] and (5) they have long half time of excretion and poor selectivity to targeting sites which tend to accumulate in the skin and eyes, leading to phototoxicity and photosensitivity for prolonged times.[13,14,113] The nonselective uptake by other cells and tissues mitigates the therapeutic efficacy of PDT. Therefore, many research groups are working actively to overcome these shortcomings by developing new nanomaterial-based photosensitizers.

3.4. QDs in Advancing $^1O_2$ Generation. The emergence of inorganic sensitizer materials, especially QDs, has yielded promising results in addressing the existing issues associated with molecular sensitizers. QDs potentially offer considerable advantages in terms of facile synthesis, size-tunable electronic and photophysical properties, broadband light absorption, high molar extinction coefficients, long luminescence lifetimes, high

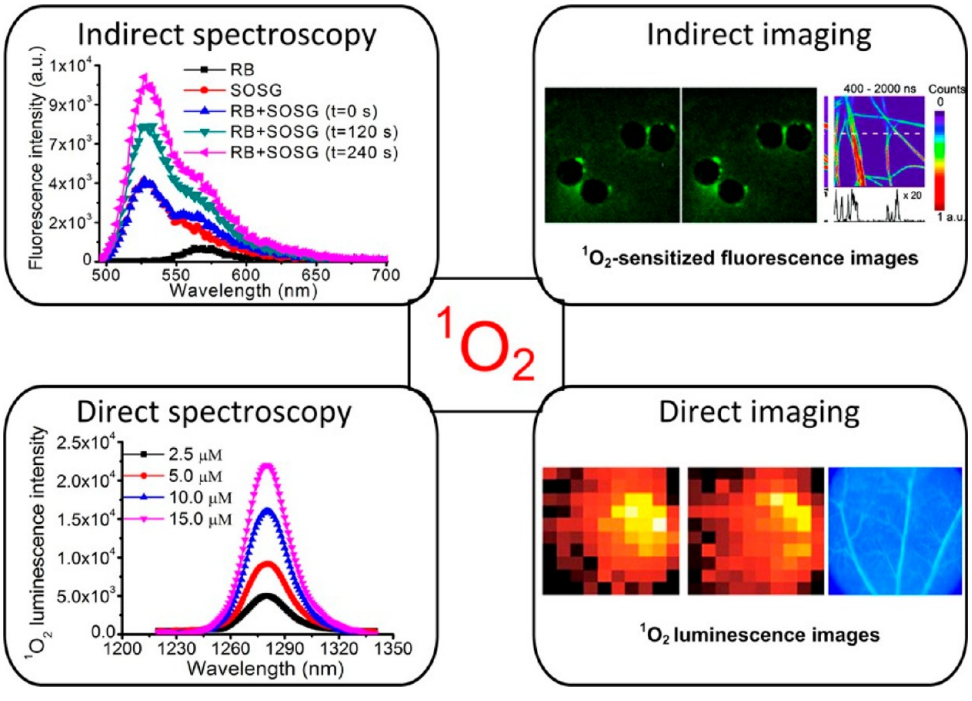

Figure 4. Direct and indirect detection of $^1O_2$ generation. Reproduced with permission from ref 111. Copyright 2016, Wiley-VCH.

https://doi.org/10.1021/acsomega.3c03962
ACS Omega 2023, 8, 34328−34353

Table 1. Summary of $^1O_2$ Generation by QDs and QD−PS Conjugates and Detection by Various Means

Quantum dots (QDs)	Light source/nm	Power density	Mode of $^1O_2$ generation	Methods of $^1O_2$ detection	QYs (%) of $^1O_2$	Target cells	ref
Blue-emitting CdSe/ZnS	400	17.57 mW cm^{-2}	TET	Phosphorescence and ERGO	18	–	5
Green-emitting CdSe/ZnS	400	17.57 mW cm^{-2}	TET	Phosphorescence and ERGO	12	–	5
Yellow-emitting CdSe/ZnS	400	17.57 mW cm^{-2}	TET	Phosphorescence and ERGO	14	–	5
ZnSe(S)	302	–	TET	SOSG	–	–	63
CuInSe/ZnS:Mn-FA	808 or 650	1 W cm^{-2}	TET	DCFH-DA	–	4T1	64
CdSe/CdS (18 nm)	white light	–	TET	ADMA and phosphorescence	25	Hela	65
CdSe/CdS (26 nm)	white light	–	TET	ADMA and phosphorescence	35	Hela	65
ZnAgInS/ZIF-8	420−780	100 mW cm^{-2}	Charge transfer	EPR	–	S. aureus and *E. coli*	67
ZnO/Au	805−860	0.1 W cm^{-2}	Charge transfer	ABDA	–	–	21
CdSe(S)	302	–	Charge transfer	SOSG	–	–	63
ZnO/CQDs	visible light	–	Charge transfer	EPR	–	–	116
CQDs/CdSe/rGO	visible light	–	Charge transfer	EPR	–	–	110
ZnO@PDA/Ag−Ag_2O	400−650	15 W	Charge transfer	EPR	–	*E. coli* and *S. aureus*	15
$NaErF_4$@ZnO	980	0.6 W cm^{-2}	Charge transfer	DCFH-DA		BHP-5-16	55
$NaYF_4$:Yb/Tm@$NaYF_4$:Yb/Er@$Zn_xCd_{1-x}S$	980	2 W	Charge transfer	ABDA	–	Hela	117
CdSe/ZnS-ZnPc	532	5 mW cm^{-2}	FRET	phosphorescence	–	–	55
CdTe/ZnS- ZnPc—R6G-FA	400 and 530	20 mW cm^{-2}	FRET	SOSG/EPR/phosphorescence	91	KB cells	43
ZnCuInS/ZnS-mTHPP	660	164.51 J cm^{-2}	FRET	–	–	B16F10-Nex2 cells and E. coli	56
CdSe/ZnS-TPP	460	3 mW cm^{-2}	FRET	SOSG	–	–	57
CdSe/ZnS-Ce6	405	–	FRET	phosphorescence	–	–	69
$CdSe_xS_{1-x}$/ZnS-ZnPc	1000	100 mW cm^{-2}	FRET	ABMDMA	–	–	70
CdSe/ZnS-TPP	460	3 mW cm^{-2}	FRET	SOSG	20	–	57
CdSe-PCA	488−600	–	TTET	phosphorescence	–	–	58
CdSe-ACA	505	1 mJ	TTET	phosphorescence	–	–	20
CdSe-PCA	505	1 mJ	TTET	phosphorescence	–	–	20
InP-QCA	400	0.2 μJ/pulse	TTET	phosphorescence	–	–	59
InP-NA	400	0.2 μJ/pulse	TTET	phosphorescence	–	–	60
$CsPbCl_3$ and $CsPbBr_3$-RhB	460	30 mW	TET	DPBF	31.8	–	66
$MAPbX_3$ (MA = CH_3NH_3, X = Br, I)	473	–	TET	phosphorescence and DPBF	34	–	62
Silica-coated Cs_3PbBr	400−700	–	TET	DPBF, EPR, MO, and carotene	–	–	61
Mn^{2+}-doped $CsPbCl_3$	365	–	Mn^{2+} detects energy transfer	Phosphorescence and 4′-MAP/N	108	–	68
MoS_2	200−1000	–	TET	EPR	–	–	118
MoS_2	400−800	100 mW cm^{-2}	TET	ABDA	–	SW480	103
MoS_2	solar light	0.4 mW cm^{-2}	Charge transfer	EPR	–	*E. coli* and *S. aureus*	77

photoluminescence quantum yields, negligible bright-to-dark exciton relaxation energy loss (i.e., anti-Stokes shift), trivial postsynthesis functionalization and modification of surface chemistry, superior photochemical stability, and high resistance to photodegradation.[5,20,42,53,54,73,89,90] As the typical energy spacing between the bright and dark states (1−15 meV) is much smaller than that between the singlet and triplet states (hundreds of meV) in the molecular system, therefore, less energy loss occurs during sensitization in inorganic QDs compared to organic counterparts.[20,40,41] The trivial postsynthesis functionalization provides the QDs with high solubility in a solvent of choice coupled with offering tens of hundreds of high affinity binding sites at the surface.[73] These binding sites can be potentially linked to the number of multifunctional moieties through the coordination of metal ions on the QDs surface or van der Waals or electrostatic interactions,[92] which enable the rational design of nanohybrids with multicomponent architectures, showing a vast array of functionalities.[42,53,114] QDs possess a single exciton; however, the multivalent bindings provide the QDs with the additional kinetic advantages of energy or charge transfer, and their rate increases linearly with the number of adsorbed molecular acceptors. Excessive consumption of oxygen and vascular shutdown during PDT results in hypoxia, thus reducing the therapeutic efficacy and preventing the full therapeutic response. Moreover, solid tumors have regions of intrinsic hypoxia because of the compromised microcirculation and decreased perfusion.[8,13,53] Therefore, QDs can act as hydrogenase-type catalysts and convert hydrogen

https://doi.org/10.1021/acsomega.3c03962
ACS Omega 2023, 8, 34328−34353

peroxide (H_2O_2), which may be present in high concentration in tumors, into $^3O_2$.[106,115] QDs provide us the opportunity to use either as an individual sensitizer of $^1O_2$ generation (via TET or charge transfer)[5,53,61−65] or by linking to some other sensitizer acceptor molecules,[21,53,63,66,67] thus acting like versatile sensitizers for $^1O_2$ generation (Table 1). The size-dependent confinement of excitons ensures the photophysics of QDs to position them strategically and selectively precise to an absorption profile of a molecular acceptor for potential energy transfer via FRET or TTET processes.[20,43,53,55−60,114] It is noteworthy that the QDs also present variable shape morphology such as spheres, wires, rods, and platelets coupled with modifiable surface chemistry by depositing different anionic- or cationic-rich inorganic materials or molecular surface ligands. These features of QDs provide a vast platform to selectively adsorb molecular acceptors through hydrophobicity, charge, size, shape, etc.[21,42,53,63,66,67] Additionally, QDs nanoformulations of PS improve the solubility, tumor cells/tissue specificity, controlled delivery, and accumulation of conjugated PS in high concentrations at the tumor masses.[113] Moreover, the smaller size NCs enhance the biodistribution and prolong the circulation time and enable tumor targeting either by active targeting through surface modifications with specific cancer-targeting ligands or an enhanced permeation and retention effect.[8,53,113]

4. DESIGN AND MECHANISM OF QDS ENERGY TRANSFER

The type of energy transfer mechanism depends on the alignment between the conduction band (CB) of QDs and the singlet state of molecules in a donor−acceptor system. If the position of the singlet excited state of the molecular acceptor is below and close to the CB of QDs, the energy transfer can occur either by Förster energy transfer (FRET) or Dexter energy transfer (DET) to create a singlet excited state acceptor.[20,43,55−60,75] On the other hand, TET is a preferred pathway if the singlet excited state of molecules lies above the CB of QDs.[119] However, long-range dipole-based FRET, short-range DET, and electron transfer are considered dominant nonradiative pathways to transfer singlet energy in donor−acceptor (D−A) systems. The term FRET is named after Theodor Förster, a theoretical physicist who proposed an equation to quantify the energy transfer efficiency from an energy donor (D) to an acceptor (A) in 1948. FRET is a nonradiative energy transfer process from an excited state donor (D*) to a proximal ground state acceptor (A) through a long-range transition dipole moment, producing a donor in the ground state (D) and an acceptor in the excited state (A*),[75,120] shown by the following mechanism (i):

$$D^* + A \rightarrow D + A^* \quad \text{(i)}$$

The energy transfer rate constant (k_{FRET}) relies on the degree of dipole−dipole coupling (Coulombic interactions), the significant spectral overlap between the emission of the donor and absorption of the acceptor within an approximate distance between 1 and 10 nm,[120,121] and the dipole orientation of donor/acceptor species. The Förster dipole−dipole formalism in terms of rate constant can be expressed by eq 1.[121]

$$k_{FRET} = 1/\tau_D \left(\frac{R_0}{r}\right)^6 \quad (1)$$

where R_0 is the Foster radius (D−A distance where E_{FRET} is 50%); r is the distance between D and A; and τ_D is the lifetime of the donor in the absence of the acceptor. FRET follows the r^{-6} dependence; therefore, the energy transfer rate constant (k_{FRET}) decreases with increasing donor/acceptor distance to the power of − 6 ($k_{FRET} \propto r^{-6}$). The R_0 can be calculated by eq 2

$$R_0^6 = (8.79 \times 10^{-28}\text{mol}) n^{-4} \Phi_D k^2 j \quad (2)$$

where Φ_D is the fluorescence quantum yield of a D; n is the refractive index of a surrounding medium; k^2 is the dipole orientations; and j is the spectral overlap integral. FRET, being a resonant dipole coupling process, depends upon the dipole orientation between the donor and acceptor typically approximated as 2/3.[119,120] Additionally, FRET also depends upon the lifetime and QYs of the donor and the quenching efficiency of the acceptor.[121] The energy transfer efficiency (E_{ET}) of FRET can be determined by using the ratio between fluorescence intensities and the decay lifetime of the D in the presence and absence of the A, as expressed by following eq 3.[71]

$$E_{ET} = 1 - \frac{I_{DA}}{I_D} = 1 - \frac{\tau_{DA}}{\tau_D} \quad (3)$$

where I_{DA} and I_D are the fluorescence intensities and τ_{DA} and τ_D the decay lifetimes of the D in the presence and absence of the A, respectively. If the molecular acceptor exhibits fluorescence, the efficiency of FRET is measured by the decrease in the fluorescence of donors accompanied by an increase in acceptor fluorescence. However, when the acceptor is nonfluorescent, FRET results in the quenching of donor fluorescence.

On the other hand, the DET process developed by David L. Dexter in 1953 is determined by short-range intermolecular orbital overlap and proceeds via an electron exchange process between the donor/acceptor within a relatively shorter distance (1−2 nm).[120] The Dexter energy transfer coupling is generally mediated by direct two-species coupling (D*A → DA*) and sequential one-species superexchange couplings or electron transfer: D*A → D^+A^- → DA* and D*A → D^-A^+ → DA*.[122] The formalism for DET in terms of the rate constant of electron exchange can be expressed as exponential decay by eq 4:[120]

$$k_{DET} = Kje^{-2r/r_0} \quad (4)$$

DET, being rooted in electron exchange, relies on the K orbital interactions, r^0 van der Waals radii of the donor−acceptor, and j spectral overlap. However, in FRET the j is convoluted with the ε_A extinction coefficient. In contrast, the DET rate constant k_{DET} is an exponential function of the donor/acceptor distance $k_{DET} \propto e^{-2r/r_0}$.[120]

Similarly, electron transfer requires orbital overlap between D−A and depends upon the inner and outer sphere reorganization of the D−A pair and the solvent system. The theory of electron transfer was developed by Marcus in 1965. In a conventional QDs electron transfer model, the electrons on the CB are assumed to be transferred to the acceptor, while the hole remains unchanged on the VB, thus generating a charge-separated state with QDs, which eventually undergoes interfacial charge recombination to regenerate the ground state by back-electron transfer or is formally viewed as hole transfer from QDs. The formalism for nonadiabatic electron transfer is given by the following eq 5.[123]

$$k = \frac{2\pi}{\hbar} \frac{|H|^2}{\sqrt{4\pi\lambda k_B T}} \exp\left[-\frac{(\lambda + \Delta G)^2}{4\lambda k_B T}\right] \quad (5)$$

https://doi.org/10.1021/acsomega.3c03962
ACS Omega 2023, 8, 34328−34353

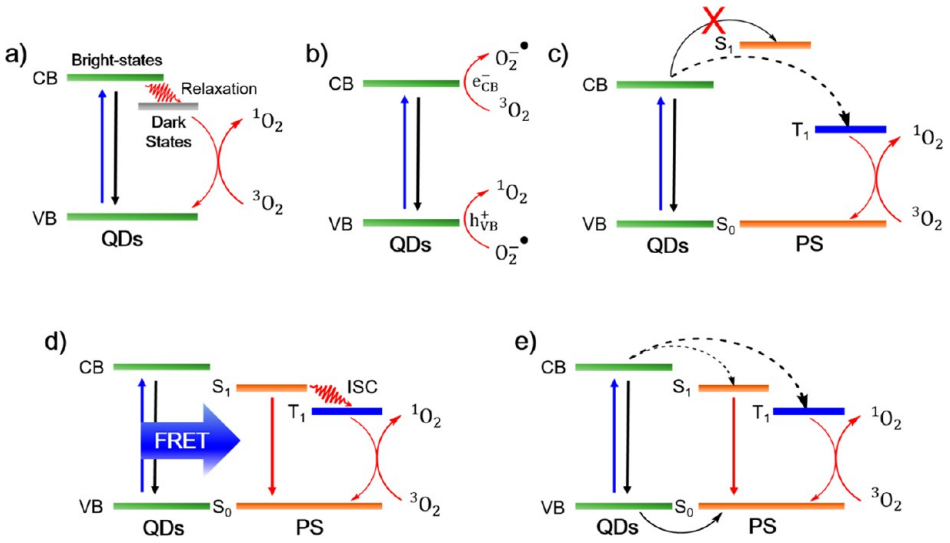

Figure 5. Jablonski diagram of energy migration from the triplet excited state of QDs to the ground state of molecular oxygen, modified from refs 5, 61, 102 (a), reduction of oxygen at the CB and oxidation of superoxide $O_2^{-\bullet}$ at the VB to produce $^1O_2$, modified from ref 67 (b), energy transfer from the QDs donor to the triplet state of the molecular acceptor, modified from refs 58−60 (c); and energy transfer from the QDs donor to molecular acceptor via either FRET or DET/sequential charge transfer (d,e), respectively, modified from refs 66, 71, 120.

where H is the electronic coupling strength; λ is the total reorganization energy for electron transfer; ΔG is the driving force; k_B is the Boltzmann constant; $\hbar$ is the Plank constant; and T is the temperature. Similar to the DET process, the electronic coupling strength is assumed to decay exponentially with D−A distance given by the following eq 6.

$$H^2 = H_0^2 e^{-\beta r} \tag{6}$$

where H_0 is the electronic coupling factor that depends upon the overlap between diabetic wave functions representing localized charges. The square moduli (H^2) of these wave functions rely exponentially on ($e^{-\beta r}$), the separation distance (r) with a prefactor and decay rate (β) which is material dependent.

5. DEVELOPMENT OF QDS-BASED SENSITIZERS

QDs nanomaterials can sensitize the $^1O_2$ by multiple mechanisms, thus acting like a versatile photosensitizer. The design of the energy transfer process is important in a QDs donor−acceptor system because it enables one to optimize the excited-state interaction and efficiently transfer energy to dioxygen.[20,43,120,53,55−60,114] QDs possess multiple channels for energy transfer to generate singlet oxygen $^1O_2$ directly or indirectly, including singlet energy transfer, triplet energy transfer, surface trap energy transfer, and electron transfer from QDs. Furthermore, QDs materials can generate $^1O_2$ directly by molecular-like sensitization via TET[5,53,61−65] (Figure 5a) or indirectly by charge transfer[21,63,66,67] (Figure 5b). For example, in the QDs under irradiation, the electrons are promoted to the CB, while holes are left behind on the VB, creating an electron−hole pair (exciton) or singlet excited state. The QDs then undergo relaxation via the ISC process (in the language of molecular sensitizer) to convert singlet excitons to triplet excitons which interact with $^3O_2$ producing $^1O_2$ via TET[5] (Figure 5a), or the electrons on the CB interact with $^3O_2$ and produce $O_2^{-\bullet}$ which is subsequently oxidized by the holes on the VB to yield $^1O_2$[21] (Figure 5b). In another strategy, QDs are linked to some other organic PS by electrostatic interaction or covalent bonding, producing a QDs−PS hybrid nanostructure (Figure 5c−e) which operates as an energy donor fluorophore (QDs) and ground state acceptor molecule (PS).[20,43,55−60,75]

Since direct excitation of a PS triplet state is spin forbidden, the PS singlet excited state undergoes ISC or singlet fission to produce triplet excited states.[120] Alternately, molecular triplet states are populated by strategically placing the bandgap of QDs smaller than the singlet excited state of the acceptor but greater than its triple excited state[19,58] (Figure 5c). Thus, QDs due to small energy spacing between bright states and dark states have mixed single/triplet character and can be expected to undergo energetically favorable singlet/triplet energy transfer to triplet excited states (Figure 5c) of the molecular acceptor.[19,20,58,120] Similarly, for singlet energy transfer, the bandgap of QDs is placed higher than the singlet excited state of the molecular acceptor (Figure 5d,e). Such energy transfer is accomplished via either FRET or DET or sequential charge transfer (Figure 5d,e) depending on the spectral overlap and distance between donors and acceptors.[120] Thus, these unique features of $^1O_2$ generation can enable the QDs superior nanophotosensitizers over the molecular and nanomaterial-based photosensitizers including the polymeric, plasmonic, metallic, and ceramic NPs, etc.

5.1. Generation of $^1O_2$ by Semiconductor QDs.

Semiconductor QDs have been reported to generate $^1O_2$ by multiple mechanisms, either individually, i.e., via triplet energy transfer (TET) and charge transfer, or in conjugated form with other inorganic materials or molecular sensitizers, i.e., via Förster resonance energy transfer (FRET) and Dexter-like energy transfer (DET) or sequential triplet−triplet energy transfer (TTET).

5.1.1. Triplet Energy Transfer (TET). Quantum dots have been treated as potential molecular sensitizers, due to their unique singlet-/triplet-like behavior.[5,20,58,124] These unique features endow the QDs with excellent catalytic properties for the generation of $^1O_2$ via energy transfer from the triplet excited state of QDs to the ground state of triplet oxygen. The QDs application as a sensitizer for $^1O_2$ generation via TET was initially proposed by Samia et al. in 2003 between the photoexcited CdSe compound and $^3O_2$ in toluene, which was confirmed by decay emission at 1270 nm. They were able to

https://doi.org/10.1021/acsomega.3c03962
ACS Omega 2023, 8, 34328−34353

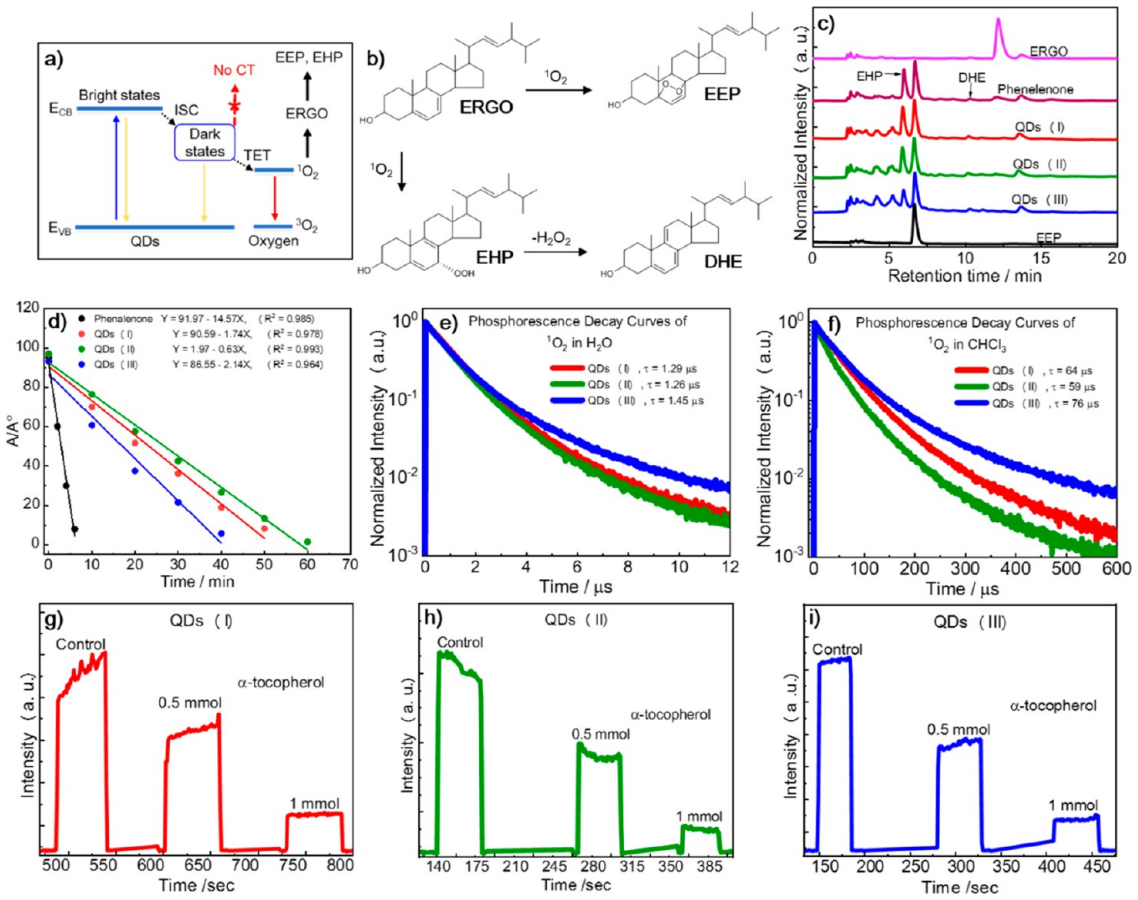

Figure 6. Detection of $^1O_2$ formation indirectly by the chemical trapping method and directly by spectroscopic analyses for yellow-emitting QDs (I), green-emitting QDs (II), and blue-emitting QDs (III). Jablonski diagram of $^1O_2$ generation by QDs (a). Reaction of $^1O_2$ with ERGO produced EEP and EHP (b). HPLC analyses of the decomposition of ERGO and production of EEP and EHP after reacting with $^1O_2$ generated by QDs and phenalenone (standard photosensitizer) (c). Rate constants of ERGO decomposition (d). Phosphorescence decay curves of $^1O_2$ in water (e) and chloroform (f). Detection of $^1O_2$ quenching in the steady state in the presence of α-tocopherol and QDs (I) (g), QDs (II) (h), and QDs (III) (i) by a photomultiplier. The figures (f–h) show the signal from $^1O_2$ without α-tocopherol (control) and in the presence of different concentrations of α-tocopherol. Adopted with permission from ref 5. Copyright 2023, American Chemical Society.

produce $^1O_2$ directly by CdSe quantum dots independently without the involvement of traditional PS or indirectly linking to PS (e.g., phthalocyanine: Pc4).[124]

The efficiency of the QDs energy migration to dioxygen depends upon the composition and photoluminescence properties of nanocrystals. For example, we studied yellow-, green-, and blue-emitting CdSe/ZnS QDs having various interfacial alloy compositions and different shell thicknesses for $^1O_2$ generation efficiency in the light without linking to molecular sensitizers.[5] The different yellow-, green-, and blue-emitting CdSe/ZnS QDs were labeled as QDs (I), QDs (II), and QDs (III), respectively. The generation of $^1O_2$ via TET from QDs to $^3O_2$ (Figure 6a) was analyzed using an Ergosterol compound (ERGO) as an $^1O_2$ scavenger and phenalenone as a standard photosensitizer. ERGO is known to react with $^1O_2$ in a Deils–Alder cycloaddition reaction, forming ergosterol-5,8-endoperoxide (EEP) and ergosterol 7-hydroperoxide (EHP) (Figure 6b). Thus, the appearance of characteristic EEP and EHP peaks in the HPLC chromatogram confirms the reaction of $^1O_2$ with ERGO (Figure 6c). The molecular-like sensitization of QDs was suggested to be responsible for TET to the ground state of oxygen, forming $^1O_2$.

The QDs showed different $^1O_2$ generation efficiencies, which were attributed to the difference in the shell thickness and quantum confinement effect. The $^1O_2$ quantum yields by using the QDs as a photosensitizer were calculated from the rate constants (Figure 6d) of ERGO decomposition as 0.14, 0.12, and 0.18% for yellow-, green-, and blue-emitting CdSe/ZnS QDs (I, II, and III), respectively. The blue-emitting QDs (III) exhibited comparatively higher QYs because in terms of downhill driving force the excited state of the QDs sensitizer can transfer energy effectively by positioning itself higher than the lower energy state of the acceptor.[58,98,125] On the other hand, lower QYs for green-emitting QDs were attributed to the excessive passivation of CdSe by ZnS. It was previously reported that a thick shell of ZnS over CdSe creates a barrier that diminishes the energy transfer.[97]

The generation of singlet oxygen was also detected by measuring the lifetimes from the luminescence decay curves based on the $^1O_2$ phosphorescence at 1270 nm under irradiation at 400 nm with a LED as a light source. We found different decay values for singlet oxygen in water and chloroform, which were found to be consistent with that for the $^1O_2$ previously reported at 3.5 μs (in water)[7] and 215 μs (in chloroform).[5] The observed different lifetimes of $^1O_2$ in water and chloroform (Figure 6e,f) were attributed to a different energy transfer from electronic states of $^1O_2$ to vibrational states of solvent molecules. The $^1O_2$ generation via TET was further confirmed by using α-

https://doi.org/10.1021/acsomega.3c03962
ACS Omega 2023, 8, 34328–34353

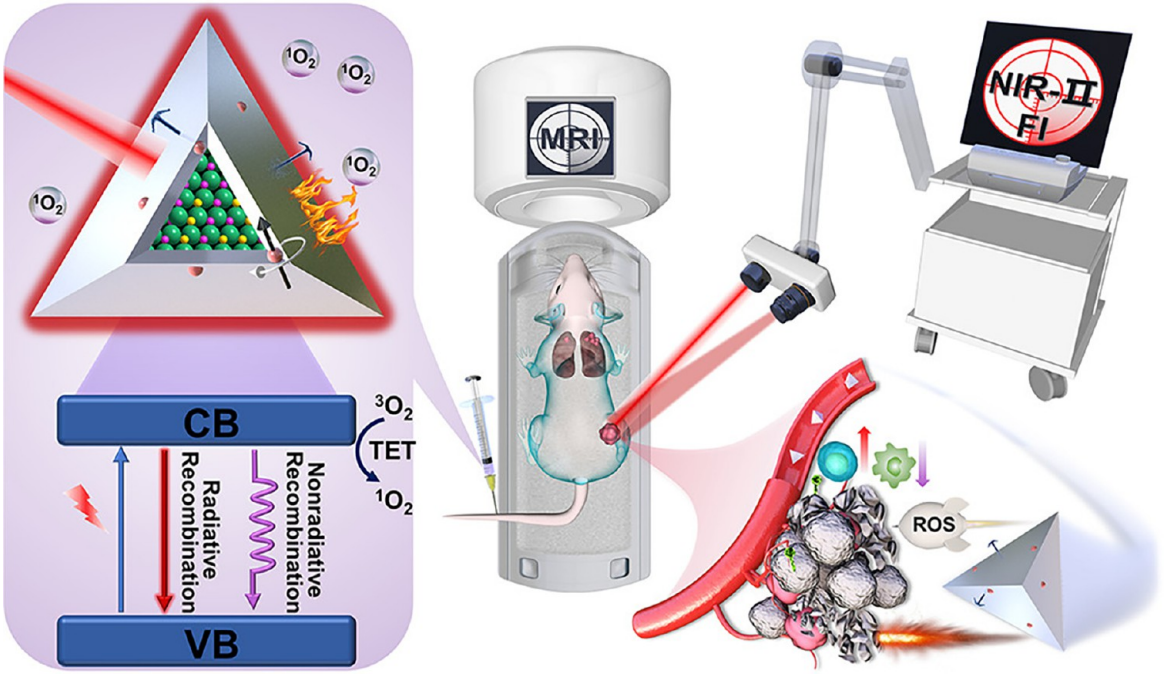

Figure 7. Schematic illustration of the QD-FA probe-assisted visualization of tumor regions and antitumor therapeutic performance in BALB/c mice. The QD-FA probe was used to visualize the tumor through fluorescence and MRI dual-modularity imaging and simultaneously employed for therapy via built-in multifunctionality, i.e., photothermal therapy and $^1O_2$-promoted photodynamic therapy. Reproduced with permission from ref 64. Copyright 2022, American Chemical Society.

tocopherol, which acts as a scavenger of $^1O_2$. It was observed that the signal ($\lambda_{emission}$ = 1270 nm) from $^1O_2$ was quenched by increasing the amount of α-tocopherol (Figure 6g–i).

The $^1O_2$ generation is also strongly dependent on the type of doping species, surface chemistry, and concentration of QDs. For example, Bailón-Ruiz and Perales-Pérez[63] synthesized cadmium (or zinc) selenide (or sulfide) systems such as CdSe(S), ZnSe(S), and Cu-doped ZnSe(S) QDs (water-soluble) of different compositions and surface chemistry and studied their capability of $^1O_2$ generation. It was observed that ZnSe(S) produced $^1O_2$ via TET, and its efficiency was enhanced after doping with the Cu^{2+} ion. However, the $^1O_2$ generation by CdSe(S) was supposed to be due to energy or electron transfer.[63] The combination of the triplet-sensitization properties of QDs with other different functional moieties introduces additional properties to the resulting system, which serves as both diagnostics and therapeutics. For example, Li et al.[64] developed a folic acid (FA) functionalized theranostic QDs probe containing NIR-II emissive CuInSe core and a Mn-doped ZnS outer shell to sensitively visualize the tumor through fluorescence and MRI dual-modularity imaging and for simultaneous use for therapy via built-in multifunctionality. The photoexcited CuInSe (labeled as CISe) and CuInSe@ZnS:Mn (CISe@ZnS:Mn) QDs produced $^1O_2$ via the TET process[64] which along with photothermal therapy (PTT, heat generated due to nonradiative relaxation pathways) was used to eliminate and prevent tumor growth in 80% of BALB/c mice (Figure 7). The FA endowed the QDs to preferentially target the 4T1 tumor cells in mice. Hence, the nanoplatforms exhibited high-performance NIR-II fluorescence and MRI dual-modality imaging and displayed excellent therapeutic efficacy.[64]

The QD-FA probe showed outstanding antitumor therapeutic performance (Figure 8a–h) in mice bearing 4T1 tumors of ~ 100 mm^3 under 808 or 650 laser irradiation compared to QD-FA treatment without laser irradiation (which exhibited a 7.2-fold increase), PTX-treated groups (8-fold increase), a PBS group (10.8-fold increase), and a PBS group followed by 808 or 650 nm laser irradiation (9.4-fold and 10.5-fold increases, respectively).[64]

The engineering of QDs with different morphologies, i.e., one-, two-, and three-dimensional geometries, endows nanocrystals (NC) with novel photophysical and photochemical features. He et al.[65] fabricated CdSe/CdS dots and rods of 18 and 26 nm which showed two- and three-photon absorption action cross sections at 800 and 1300 nm biological I and II windows, respectively. The CdSe/CdS dots/rods, under white light irradiation, produced an efficient $^1O_2$ via the TET process with QYs of 25 and 35% for nanocrystals of 18 and 26 nm, respectively, compared to those of bare spherical CdSe (5% in toluene solution).[65] The QDs showed the upconversion phenomenon with excellent two-photon-excited photodynamic therapy effect against HeLa cancer cells, under excitation at 800 nm (1 W cm^{-2}).

5.1.2. Charge Transfer. Since the recombination of photogenerated charge carriers competes with the interfacial electron transfer, the QDs can transfer electrons or holes to surface-bound molecules which leads to the formation of intermediates followed by stable products. For example, electrons in the conduction band (e^-_{CB}) are reduced with dissolved oxygen to produce superoxide $O_2^{-\bullet}$ intermediate species, which are subsequently oxidized with holes in the valence band (h^+_{VB}), generating singlet oxygen ($^1O_2$), as shown by mechanism (ii).

$$QDs + h\upsilon \rightarrow h^+_{VB} + e^-_{CB}$$

$$e^-_{CB} + O_2 \rightarrow O_2^{-\bullet}$$

$$h^+_{VB} + O_2^{-\bullet} \rightarrow {}^1O_2 \quad \text{(ii)}$$

https://doi.org/10.1021/acsomega.3c03962
ACS Omega 2023, 8, 34328−34353

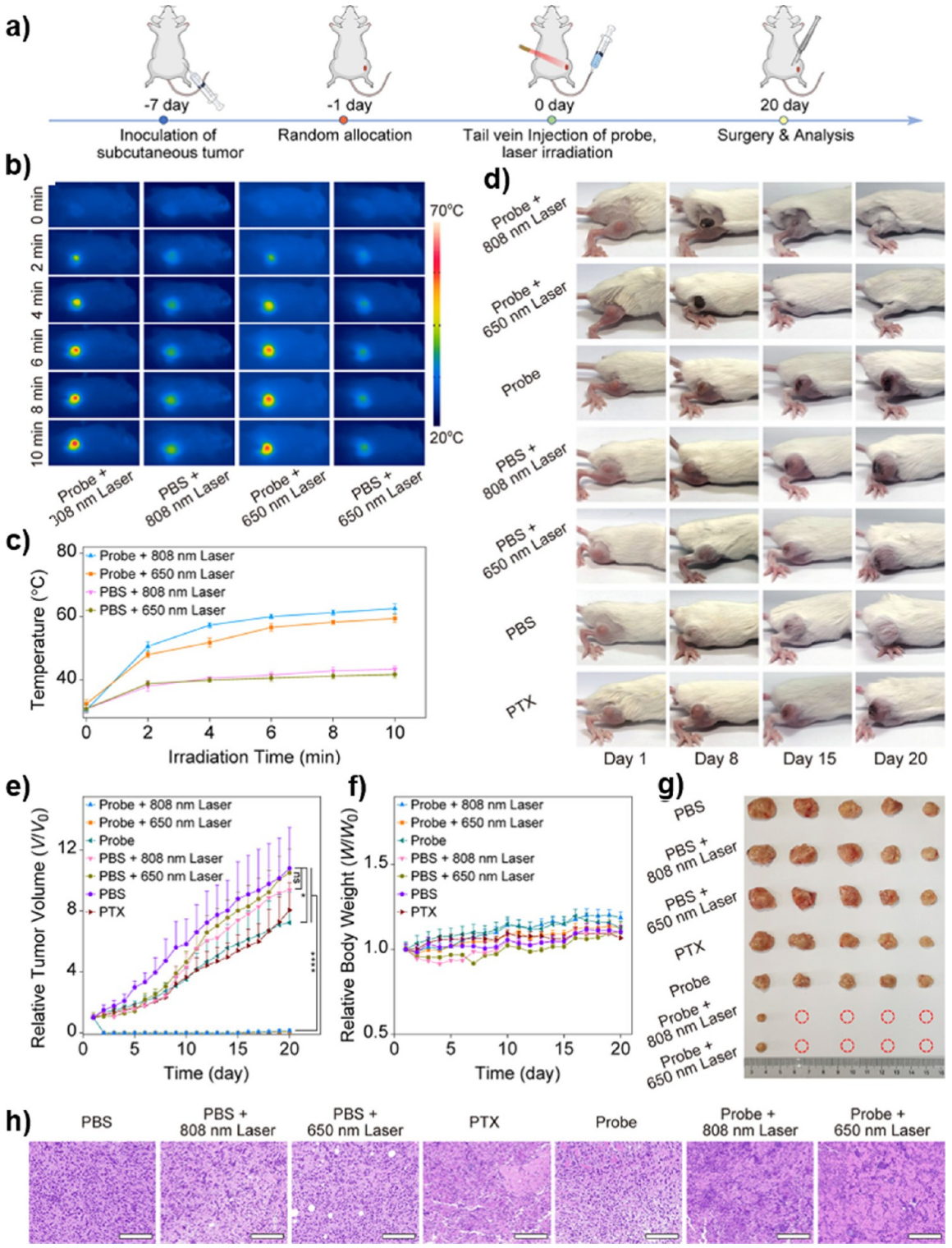

Figure 8. Antitumor therapeutic performance of the QD-FA probe *in vivo*. Schematic illustration of QD-FA probe-assisted antitumor PTT and PDT (a). Thermal images of tumor-bearing mice, injected with PBS or the QD-FA probe, were recorded after irradiation under 808 nm laser (1.0 W cm^{-2}, 10 min) and a 650 nm laser (1.0 W cm^{-2}, 10 min) for different time intervals (b). The observed temperature changes at the tumor area during the laser irradiation (c). Photographs of tumor-bearing mice after receiving intravenous injections of the QD-FA probe, the QD-FA probe with subsequent 808 or 650 nm laser irradiation, PBS, PBS with subsequent 808 or 650 nm laser irradiation, and paclitaxel (PTX) (d). Relative tumor volumes (e) and body weight of tumor-bearing mice (f) after various treatments. Representative images of tumor tissues harvested from each group, as indicated, after treatment for 20 days (g). Histological staining of tumor tissues harvested after 1 day of treatment (h). Reproduced with permission from ref 64. Copyright 2022, American Chemical Society.

Wang et al.[67] fabricated successfully GSH-capped ZnAgInS (ZAIS) QDs encapsulated with metal−organic frameworks (ZIF-8). The MOFs and ZAIS QDs nanocomposites (QDs@ZIF-8) were observed to produce efficient $^1O_2$ under visible light

https://doi.org/10.1021/acsomega.3c03962
ACS Omega 2023, 8, 34328−34353

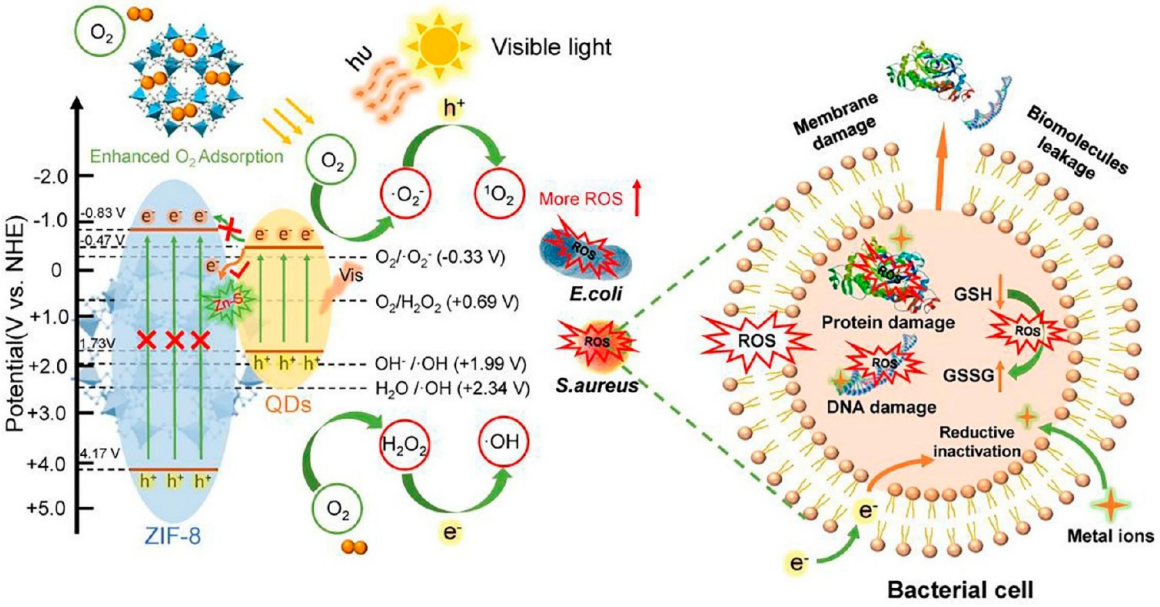

Figure 9. Schematic illustration of a photogenerated electron−hole pair, formation of $^1O_2$ and ROS, and antibacterial mechanism of the QDs@ZIF-8 probe under visible-light irradiation. Reproduced with permission from ref 67. Copyright 2021, Elsevier.

(Figure 9). It was found that the photogenerated e^-_{CB} interacted with dioxygen adsorbed on the surface of QDs@ZIF-8 to produce $O_2^{-\bullet}$ that was subsequently oxidized with h^+_{VB}, producing $^1O_2$ (Figure 9). The Zn−S bonds between QDs and ZIF-8 acted as electron-trapping sites which inhibited carrier recombination, leading to a further increase in $^1O_2$ and ROS generation. The QDs@ZIF-8 exhibited excellence antibacterial performance against *S. aureus* and *E. coli* under visible-light irradiation by destroying the bacterial cell membrane, degrading the intracellular biomolecules such as DNA and protein and oxidizing GSH.[67]

5.1.3. QDs in Combination with Other Inorganic Materials. Coupling of QDs with other inorganic NCs is an effective strategy to improve $^1O_2$ generation due to the mobility of interparticle charges and slower electron−hole recombination.[15,21,110,116] Quantum dots have been reported as generally weak sensitizers to produce $^1O_2$ compared to conventional molecular photosensitizers;[5] therefore, to enhance their photosensitization efficiency they are integrated with other nanocrystals such as Pt, Au, Ag, Pd, and TiO_2,[21,126] where the QDs act as a photosensitizer and the decorated NCs are utilized as a catalytic center to activate $^3O_2$ to $^1O_2$.[110] In contrast to the type II pathway, the inorganic hybrid NCs follow the type I pathway for $^1O_2$ generation. Upon light absorption, electrons are promoted to the CB where they interact with O_2 to produce $O_2^{-\bullet}$, which are subsequently oxidized by holes on the VB to yield $^1O_2$.[15,21,110,116] For instance, Zhou et al.[21] integrated core Au nanorods with a ZnO shell that acted as NIR light-activated photosensitizers. These Au nanorod/ZnO core−shells were found to demonstrate effective generation of $^1O_2$ under continuous-wave NIR light irradiation, with the thicker ZnO shells displaying higher $^1O_2$ generation efficiency. The mechanism of $^1O_2$ generation was attributed to the injection of NIR light-excited hot electrons of Au nanorods into the CB of ZnO (Figure 10a). The injected electrons were scavenged by dioxygen to form $O_2^{-\bullet}$ which was subsequently oxidized (Figure 10b) by the holes on Au nanorods to form $^1O_2$.[21]

Another strategy of enhanced $^1O_2$ generation is to use QDs conjugated with carbon-based nanomaterials, which have diverse applications including nanophotonics, nanoelectronics, and nanotheranostics. Quantum dots containing the largest bandgap require high-energy excitation which limits their widespread applications. Therefore, architecting QDs heterostructures by coupling with low-energy photoexcitation materials can provide promising optical results. Li et al.[116] synthesized carbon quantum dot (CQD) modified ZnO hybrid materials (CQDs/ZnO), and their dispersity was improved by loading on halloysite nanotubes (Figure 10c). The hybrid materials were found to produce efficient $O_2^{-\bullet}$ and $^1O_2$ under UV−visible excitation.[116] It was observed that under visible-light irradiation the photogenerated electrons in the HOMO level could be promoted to the LUMO level of CQDs and then transferred to the conduction band of ZnO where they interact with dioxygen, producing the $O_2^{-\bullet}$ and $^1O_2$ species (Figure 10c). The nanohybrids were observed to exhibit very high photocatalytic degradation activities against tetracycline hydrochloride (TC·HCl).[116]

Similarly, Huo et al.[110] fabricated composites of CQDs/CdSe/reduced graphene oxide (rGO) with enhanced photocatalytic activities for TC·HCl. It was observed that the introduction of rGO enhanced the charge transfer rate, thus producing more ROS such as $HO^\bullet$, $O_2^{-\bullet}$, and $^1O_2$. The proposed mechanism for $^1O_2$ was described as an electron−hole pair generated in CdSe after visible-light irradiation. The CdSe transfers the photoelectrons via CQDs to the surface of rGO where they interacted with O_2 to form the $O_2^{-\bullet}$; meanwhile, CQDs also generated electron−hole pairs, enhancing the yields of $HO^\bullet$ and $O_2^{-\bullet}$. Subsequently, the $O_2^{-\bullet}$ interacted with holes at the conduction band and generated $^1O_2$.[110]

QDs optoelectronic properties can be tailored to have n-type or p-type characters, which can be coupled with other n-type or p-type materials to construct a p−n heterojunction, thus restraining the recombination of the electron−hole pair and enhancing the ROS generation efficiency. Guo et al.[15] coupled

https://doi.org/10.1021/acsomega.3c03962
ACS Omega 2023, 8, 34328−34353

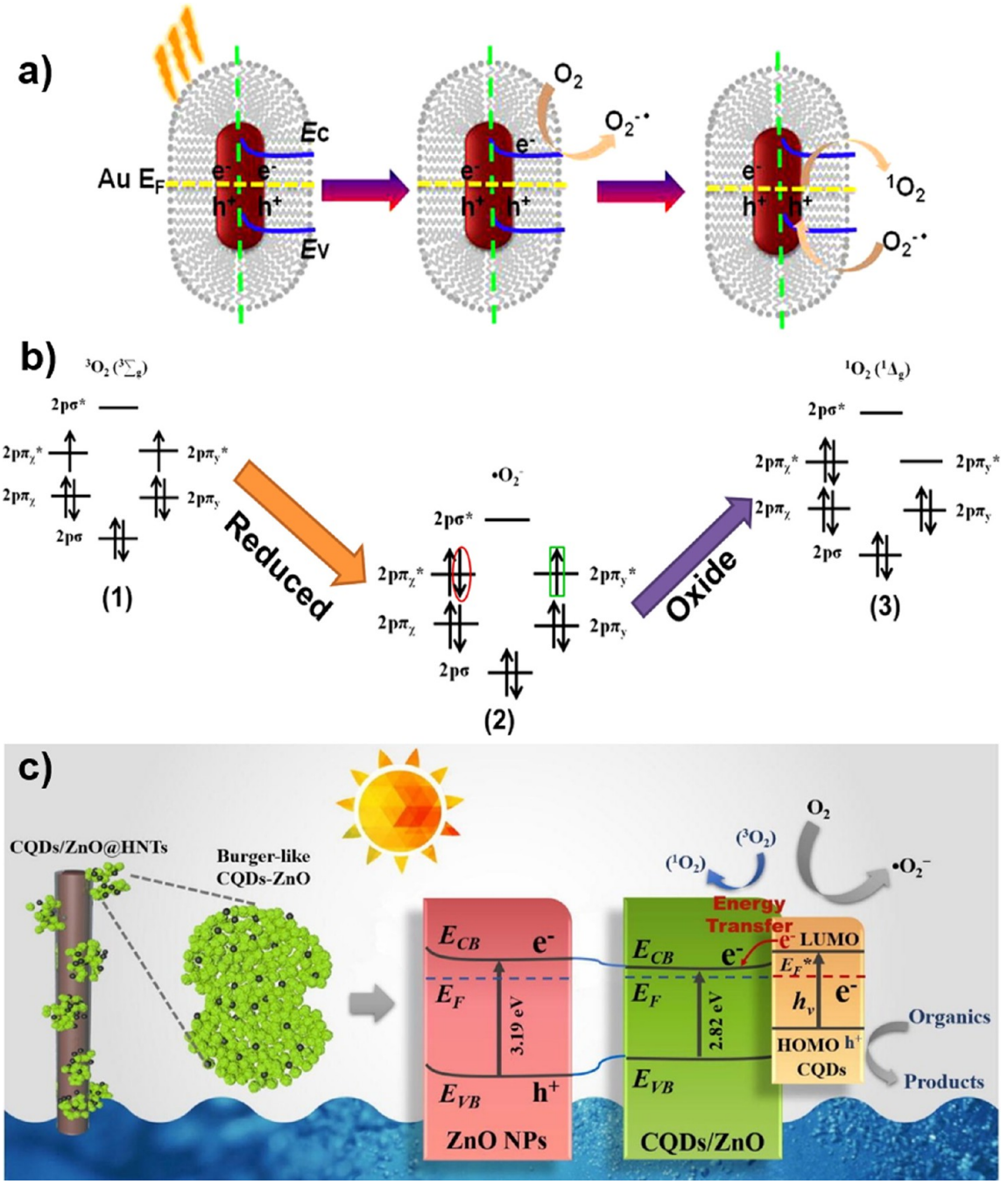

Figure 10. Schematic illustration of charge separation in Au nanorod/ZnO and mechanism of $^1O_2$ generation by the nanoconjugates (a) and the corresponding electronic structure configuration (b) under NIR light irradiation. Reproduced with permission from ref 21. Copyright 2018, American Chemical Society. Schematic illustration of the band structure, charge separation in CQD/ZnO@HNTs, and mechanism of $^1O_2$ and ROS generation by nanohybrids under visible irradiation (c). Reproduced with permission from ref 116. Copyright 2019, Elsevier.

an n-type ZnO core with p-type Ag−Ag_2O by polydopamine (PDA) to construct core−shell nanocomposites with a p−n heterojunction. Interestingly, the light absorption capacity of ZnO was remarkably enhanced after surface modification by PDA/Ag−Ag_2O nanoparticles and ZnO@PDA/Ag−Ag_2O which were found to yield a high amount of $^1O_2$ compared with unmodified ZnO and ZnO@PDA nanosheets. Upon LED irradiation of ZnO@PDA/Ag−Ag_2O, the Ag_2O nanoparticles were excited to generate the h^+_{VB} and e^-_{CB} pair. The e^-_{CB} in the CB of Ag_2O was subsequently transferred to the CB of ZnO due to the inner electric field existing in the p−n junction. Meanwhile, the PDA acted as a sensitizer, and the Ag nanoparticles worked as electron transfer mediators in this process. The CB of ZnO possesses more negative energy (−0.36 eV) than the $O_2/O_2^{-\bullet}$ potential (−0.33 eV); therefore, the e^-_{CB} in the CB reacted with O_2 to generate the $O_2^{-\bullet}$. The $O_2^{-\bullet}$ subsequently interacted with h^+_{VB} in the VB of Ag_2O, producing a high amount of $^1O_2$ (Figure 11A).

The nanocomposites exhibited superior disinfection efficiency under irradiation against *E. coli* and *S. aureus*. To validate the disinfection ability of nanocomposites *in vivo*, *S. aureus* was inoculated into the back skin of Kunming mice. The ZnO@

https://doi.org/10.1021/acsomega.3c03962
ACS Omega 2023, 8, 34328−34353

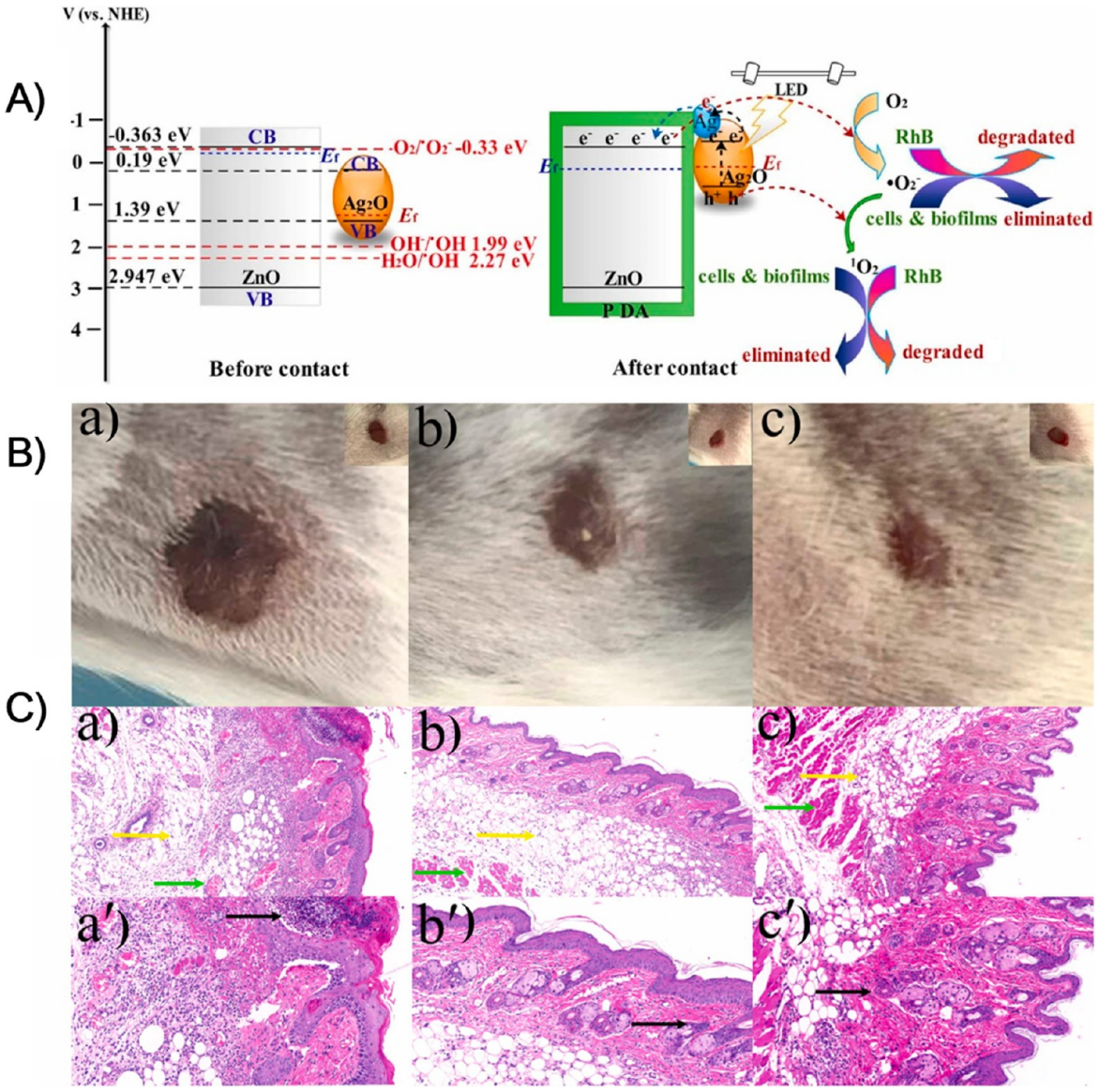

Figure 11. Schematic illustration of band structure alignment, charge separation in ZnO@PDA/Ag−Ag_2O, and the proposed mechanism of ROS generation and photocatalytic degradation by the nanoconjugates under visible LED irradiation (A). Representative photographs of *S. aureus* infected wounds harvested after 3 days of PDT treatment (B): control (a), ZnO@PDA/Ag−Ag_2O without irradiation (b), and ZnO@PDA/Ag−Ag_2O with irradiation for 15 min (c). The insets show the wound images on the first day of treatment. H&E stained micrographs of infected mice tissues harvested after 3 days of PDT treatment (C): control (a), ZnO@PDA/Ag−Ag_2O without irradiation (b), and ZnO@PDA/Ag−Ag_2O with irradiation for 15 min (c). The bottom panel, i.e., a′, b′, c′, shows the magnified partial version of a, b, and c. Black arrows: inflammatory cells; green arrows: red blood cells; and yellow arrows: vacuolization. Reproduced with permission from ref 15. Copyright 2022, Elsevier.

PDA/Ag−Ag_2O under LED irradiation effectively minimized the bacterial growth and accelerated wound healing (Figure 11B,C) due to the $^1O_2$ generated by the nanocomposites coupled with the release of Ag nanoparticles, as compared with the control and ZnO@PDA/Ag−Ag_2O without irradiation.[15]

Since NIR light has high tissue penetration capability, sensitizers with excitation in the NIR window are the primary consideration for potential application in PDT treatment. Based on this concept, a system of $NaErF_4$@ZnO upconversion nanoparticles (UCNPs) was designed by overcoating blue- (415 nm), green- (525/545 nm), and red-emitting (661 nm) $NaErF_4$ UCNPs with ZnO. Upon excitation by 980 nm NIR irradiation, the UV emission from $NaErF_4$-sensitized ZnO catalyzed H_2O_2 and O_2 to produce $^1O_2$ by energy transfer. The $NaErF_4$@ZnO UCNPs showed 59% cell lethality against thyroid tumor cells (BHP 5−16 cells).[51] Similarly, Wang et al.[117] fabricated $NaYF_4$:Yb/Tm@$NaYF_4$:Yb/Er UCNPs which were subsequently passivated by $Zn_xCd_{1-x}S$ quantum dots. The UCNPs/$Zn_xCd_{1-x}S$ were excited with NIR light from solar energy, which further activated the $Zn_xCd_{1-x}S$ via the FRET or irradiation energy transfer (IET) process to produce a photogenerated electron−hole pair. The resulting activated UCNPs/$Zn_xCd_{1-x}S$ were observed to exhibit a high production ability of $^1O_2$ and $HO^•$.[117]

5.1.4. QDs-Conjugated Sensitizers. A QD-conjugated photosensitizer (QD-PS) has been broadly used by many research groups to maximally harvest the energy of QDs for indirect $^1O_2$ generation. In a QD-PS system, the QDs in the excited state energy transfer to the surface-anchored molecular acceptor/sensitizer via Förster resonance energy transfer

https://doi.org/10.1021/acsomega.3c03962
ACS Omega 2023, 8, 34328−34353

(FRET)[43,55−57,69−71] or Dexter-like energy transfer (DET) processes or sequential triplet−triplet energy transfer (TTET).[58−60] The molecular sensitizer subsequently transfers its energy nonradiatively to the ground triplet-state oxygen generating $^1O_2$.[43,55−60,69−71]

Förster Resonance Energy Transfer (FRET). The concept of indirect $^1O_2$ generation can be better explained by a study performed by Monte et al.[71] The authors developed a system of CdSe/ZnS QDs as an energy donor and zinc-phthalocyanine (ZnPc) as an energy acceptor, which is a sensitizer of $^1O_2$ generation (Figure 12). The FRET efficiency of the QD-ZnPc

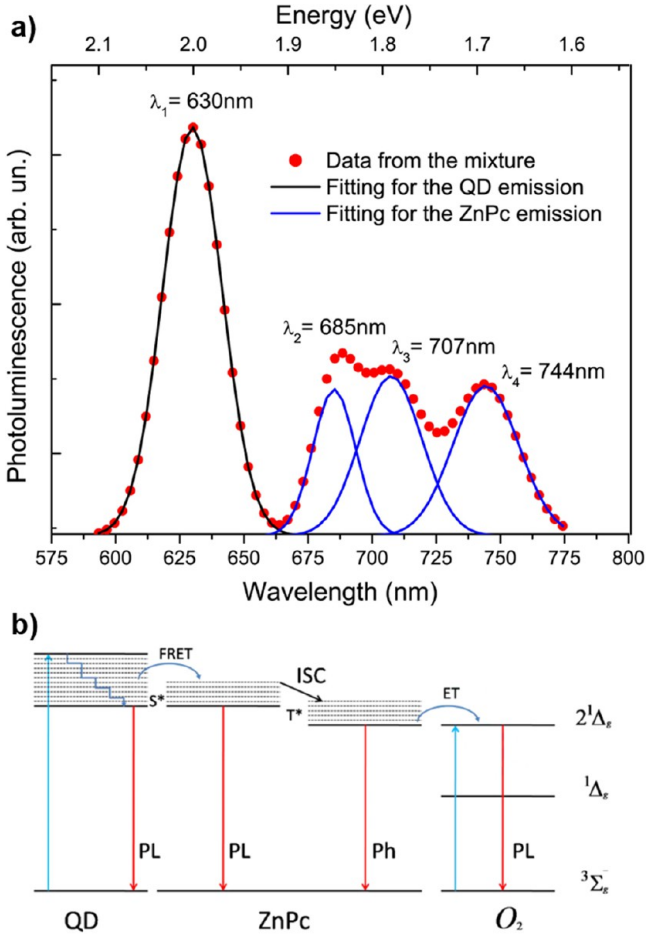

Figure 12. Photoluminescence spectra of CdSe/ZnS-ZnPc (a). The multipeak Gaussian fitting shows four emission peaks from QDs (630 nm), ZnPc (685 and 744 nm), and $^1O_2$ (707 nm). Jablonski energy diagram representation of energy transfer from QDs to ZnPc and ground state molecular oxygen, producing $^1O_2$: PL (photoluminescence), ISC (intersystem crossing), Ph (phosphorescence), and ET (energy transfer). Reproduced with permission from ref 71. Copyright 2020, Wiley-VCH.

was measured by the relative decrease in the photon diffusion length at an emission wavelength of 630 and 707 nm, using the microluminescence scan surface technique (MSST). In sequence, QDs at different concentrations were mixed with a fixed amount of ZnPc to produce a FRET nonradiative process. A decrease in the photon diffusion length was observed when the QDs and ZnPc came closer to each other to a distance of 1−10 nm, signifying the occurrence of FRET. Hence, in a cascade-like process, the QDs transferred their energy to ZnPc, and in turn, ZnPc excited $^3O_2$, generating $^1O_2$ (Figure 12). The photoluminescence of QD-ZnPc exhibited four different emission peaks arising from QDs (630 nm), ZnPc (685 and 744 nm), and $^1O_2$ (707 nm).[71]

Moreover, the PS accumulation at the tumor area is remarkably important in cancer treatment by PDT. Therefore, the surface modifications of QDs with specific cancer-targeting ligands enable them to evade the reticuloendothelial system (RES) and achieve the maximum concentration of PS at tumor masses by active targeting. For example, Shen et al.[43] designed a unique CdTe/ZnS QDs-Zn-porphyrin (TMPyP-Zn-QDs complexes) hybrid nanoparticle (HyNP) through micelle encapsulation with highly fluorescent organic photosensitizer rhodamine 6G (R6G) and NIR fluorophore (NIR775) by folic acid (FA) labeled amphiphilic phospholipid polymers (Figure 13a). The HyNPs were named HyNPs1 (without R6G and FA), HyNPs2 (without FA), and HyNPs3 (containing both R6G and FA). The QDs fluorescence at 560 nm acted as an energy donor, and TMPyP acted as an energy acceptor. The nanohybrids were reported to have large porphyrin payloads and strong light absorption, thus contributing to a high production of $^1O_2$ quantum yield (Φ = 0.91) compared to the standard photosensitizer Rose Bengal (Φ = 0.75). The high $^1O_2$ QY was attributed to an efficient dual-energy transfer process from the respective QDs and R6G (Figure 13b) to the *in situ* formed TMPyP-Zn in HyNPs.

In *In vivo* studies, the HyNPs demonstrated a high ability to escape RES and accumulated preferentially in tumors through folate-receptor-mediated active delivery (Figure 13c), allowing noninvasive fluorescence imaging of tumors and their ablation via PDT (Figure 14a−d), without causing noticeable side effects. After 20 days of treatment, the tumor volumes were reduced significantly in mice receiving the HyNP3 probe and light irradiation as compared to control (mice receiving either saline, HyNP1, HyNP1 + light irradiation, HyNP3, or light only).[43]

Tsolekile et al.[56] developed nanohybrids consisting of ZnCuInS/ZnS (ZCIS/ZnS) QDs and 5,10,15,20-tetrakis(3-hydroxyphenyl)porphyrin (mTHPP). The ZCIS/ZnS-mTHPP nanoconjugates exhibited the highest reduction in cell viability (72%) against the murine metastatic melanoma (B16F10-Nex2) cell line compared to bare QDs (19%) and mTHPP (1%).[56]

After the NP enrichment at the tumor area, the clinical use of PDT agents for deep tissue tumor curing remains challenging because most of the PDT agents are activated by short wavelength light which hardly travels far into biological tissues due to light-scattering effects and absorption of biological chromophores.[13] In this case, it is desirable to use photosensitization by deeply penetrating NIR light rather (lower energy) than UV−visible light (higher energy). However, the electronic energy levels of molecular sensitizers are usually higher than those of the lower energy exciting photons of NIR light. Therefore, the PDT activity in such a case can be obtained by coupling molecular sensitizers to other strongly multiphoton-absorbing species. Drozdek et al.[70] developed biocompatible polymer nanocapsules loaded with two-photon absorption excited (800−1000 nm) $CdSe_xS_{1-x}$/ZnS and zinc(II) phthalocyanine (ZnPc) as a simple hybrid system for demonstrating bioimaging, energy transfer, and potential PDT applications. The absorption spectrum (650−750 nm) of the ZnPc acceptor overlapped quite precisely with the emission spectrum (658 nm) of the QDs donor, which exhibited 16−19% FRET efficiency. However, the obtained results showed that $^1O_2$ was produced about five times more by free ZnPc compared to QD-conjugated

https://doi.org/10.1021/acsomega.3c03962
ACS Omega 2023, 8, 34328−34353

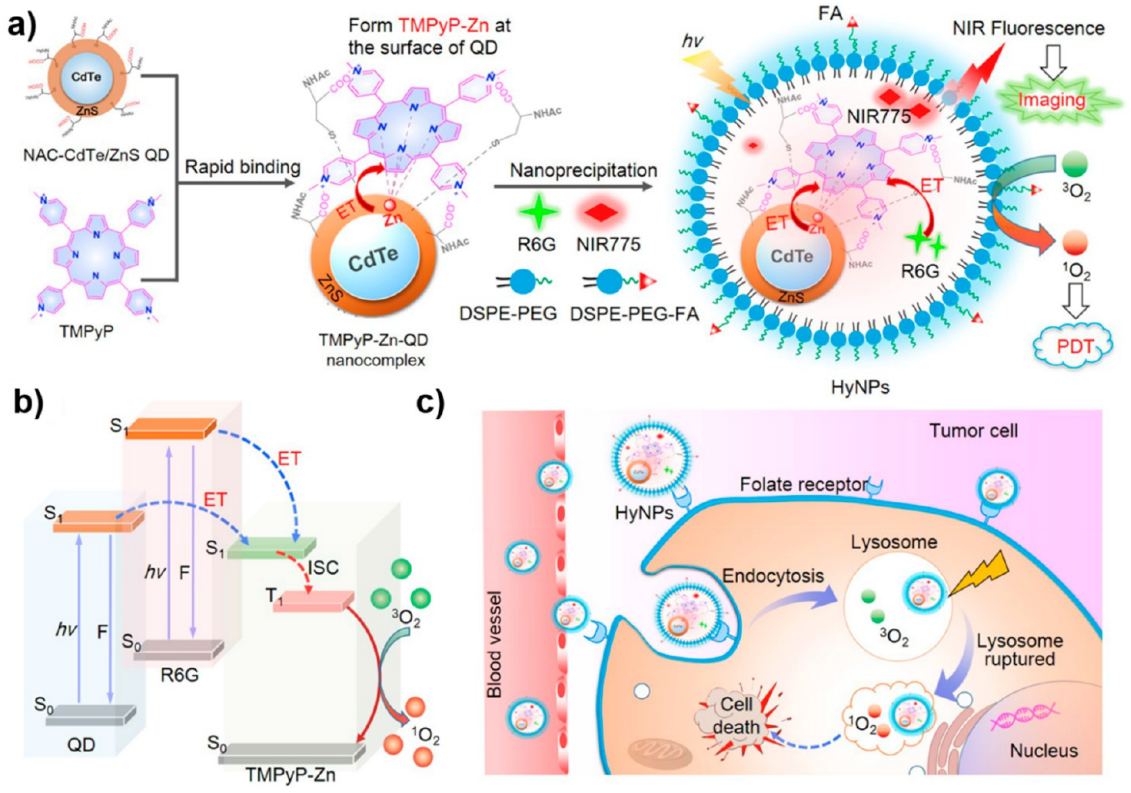

Figure 13. General design of the HyNP probe architecture consisting of preassembled unique TMPyP-Zn-QD nanocomposites, organic PS (R6G), NIR fluorophore (NIR775), and biocompatible phospholipids (a). Schematic illustration of dual-energy migration from the respective QDs and R6G to the TMPyP-Zn acceptor/sensitizer and subsequent sensitization of $^3O_2$ by TMPyP-Zn to generate $^1O_2$ (b). Schematic illustration of targeted delivery of HyNPs to tumor tissue through enhanced permeability and retention effects, cellular uptake of HyNPs through active delivery and accumulation in lysosomes, and *in vivo* PDT treatment (c). Reproduced with permission from ref 43. Copyright 2017, Elsevier.

ZnPc, probably due to the energy loss during the FRET process.[70]

Dexter-Like Energy Transfer (DET) or Sequential Triplet−Triplet Energy Transfer (TTET). Traditional approaches generally involve intersystem crossing (ISC) to transfer energy from the singlet excited state to the excited triplet state. Such a formation of ISC between singlet−triplet excited states is energy consuming (up to 1 eV in forming the triplet)[19,41] and requires UV irradiation (higher energy) due to the large energy gap between singlet and triplet states,[98,127] which limit their selectivity and usage. Recently, QD-sensitized TET has been explored as a promising route for triplet sensitization of molecular acceptors at lower energy that was previously accessible at high-energy UV irradiation.[127] The triplet exciton shows unique additional advantages including long excited-state lifetime, large exciton diffusion lengths, slow excitation energy release, and exciton migration, which make the QDs an outstanding candidate for energy donors.[58−60] QDs are excellent light-harvesting materials with a tunable absorption from the visible to near- and mid-infrared regions and have prevalent triplet excited states.[20,59,60,98,114] Therefore, significant research has been devoted to conjoining the QDs and molecular acceptor due to the realization of nonemissive triplet exciton transfer from QDs to a molecular acceptor with high efficiency in a concerted Dexter-like energy transfer (DET) or sequential triplet−triplet energy transfer (TTET).[19,41,58−60,98,120,127] In a direct DET, the QDs transfer their electron and hole to an acceptor without involving an intermediate charge transfer state, whereas the indirect or sequential energy transfer proceeds via a charge transfer intermediate.[128] A good review of the mechanistic aspects of TTET is available from the Tang and Lian groups.[128] Hence, the QDs transfers a triplet exciton to the excited triplet state of a molecular acceptor via TTET, which consequently transfers energy to $^3O_2$, thus generating $^1O_2$. Quantum dots generally have closer energy spacing (1−15 meV)[20,98,99,120] between the bright (singlet-like character) and dark (triplet-like character) exciton states and display intrinsic features of rapid/near-isoenergic spin dephasing.[127] The nearly degenerate singlet/triplet excitons give the QDs the highest triplet excited state energies among all the visible-light triplet photosensitizers (up to 3.26 eV, 380 nm).[114] These photophysical properties of QDs can be strategically positioned by tuning their particle size into the triplet energy state of the molecular acceptor for potentially transferring the exciton from the QDs to the molecular acceptor. In terms of a downhill driving force, the triplet state position of the acceptor is slightly lower than the excited triplet state of the QDs donor. Thus, the QDs with a stronger quantum confinement effect present a stronger driving force for transferring spin-triplet excitons from the band edge to molecular acceptors.[129] The resulting triplet exciton stored in the molecular acceptor can subsequently enable facile bimolecular sensitization of $^1O_2$ generation.[59] However, the close positioning of triplet states in such nanohybrids also has an inverse effect and triggers reverse TTET (rTTET), and its probability increases with the decreasing energy gap between QDs and the molecular acceptor (Figure 15), which is detrimental to the overall yield of TTET.[59] Smaller energy gaps promote a more rapid and efficient rTTET process. For instance, Mongin et al.[58] showed that in CdSe surface-anchored 1-pyrene carboxylic acid (PCA) a triplet

https://doi.org/10.1021/acsomega.3c03962
ACS Omega 2023, 8, 34328−34353

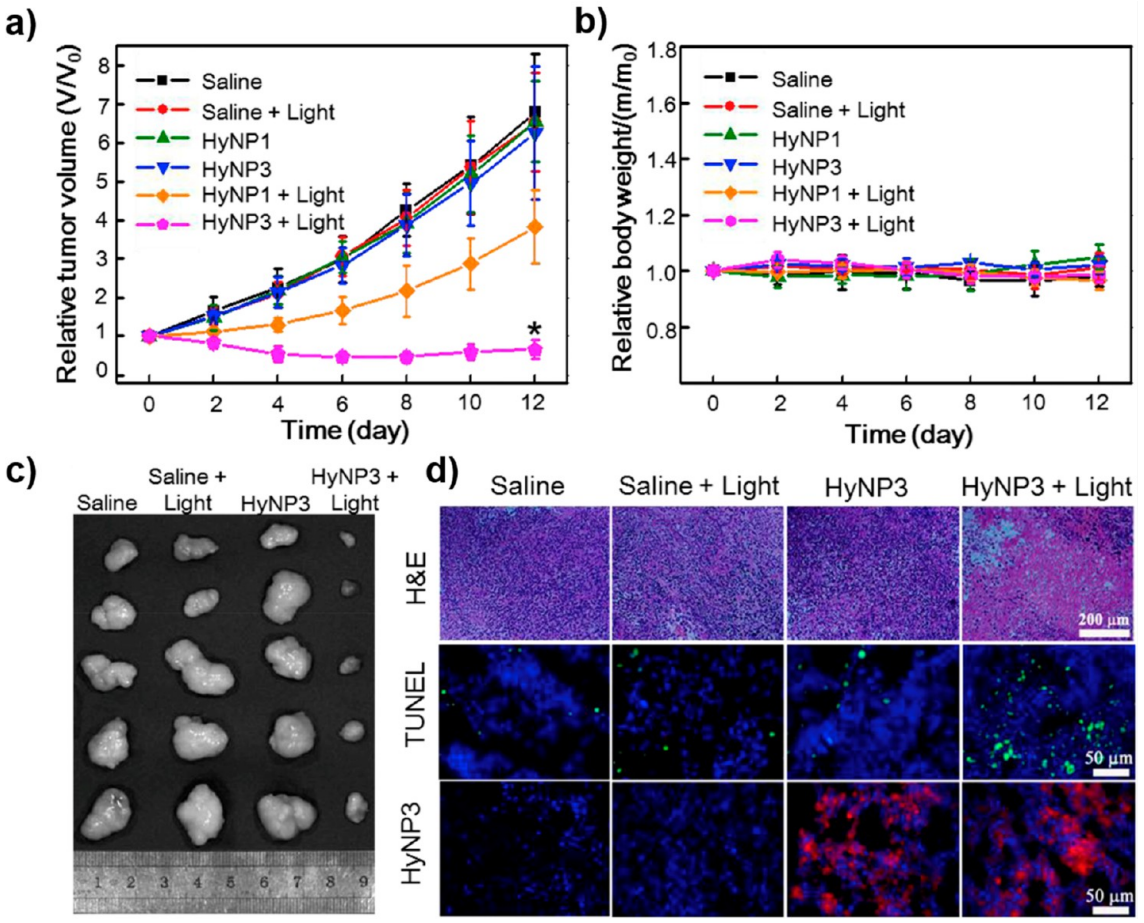

Figure 14. Antitumor therapeutic performance of the HyNP probe in tumor-bearing mice under irradiation with white light (120 mW cm^{-2}, 400 nm long pass filter) for 15 min. Changes in relative tumor volumes (a) and body weight of tumor-bearing mice (b) after 20 days of PDT treatment with either saline, saline with light, HyNP1, HyNP1 + light, HyNP3, or HyNP3 + light. Representative photographs of tumors harvested from each group, as indicated, after 20 days of treatment (c). H&E staining (up), TUNEL staining (middle), and fluorescence images (bottom) of tumor tissue slices resected from each group as indicated after treatment for 20 days (d). Reproduced with permission from ref 43. Copyright 2017, Elsevier.

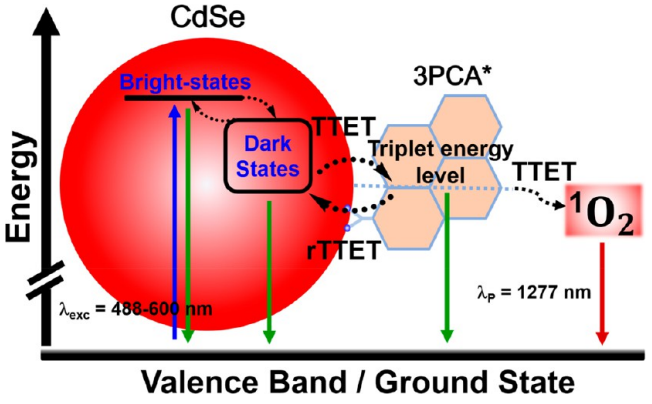

Figure 15. Schematic representation of CdSe-PCA constructs showing the associated energy levels, reverse triplet−triplet energy transfer (rTTET), various PL wavelengths, triplet−triplet energy transfer (TTET) decay pathways, and formation of $^1O_2$. Modified from ref 58.

exciton transfers backward to CdSe from the molecular acceptor, producing photoluminescence, when the energy separation between the band edge of QDs and the first triplet excited state of PCA (2.00 eV) is less than 0.54 eV (Figure 15). This phenomenon is attributed to near quantitative TTET from CdSe to PCA, producing a molecular triplet state reservoir that thermally repopulated the photoluminescent state of QDs through endothermic rTTET. However, in the presence of oxygen-saturated conditions, the QDs photoluminescence led to a dramatic decrease in intensity due to very efficient energy transfer to $^3O_2$, producing $^1O_2$. The CdSe-PCA nanohybrids were suggested to be a promising candidate for oxygen photosensitization and PDT as the materials displayed no signs of photodegradation upon prolonged photolysis.[58]

In another study, Mongin et al.[20] surface-anchored CdSe as a light-absorbing triplet sensitizer with two different triplet acceptors, namely, 9-anthracenecarboxylic acid (ACA) and 1-pyrene carboxylic acid (PCA). Under green light excitation, the CdSe/ACA and CdSe/PCA sensitized triplet excitons migrate from QDs to a surface-anchored molecular acceptor which further enabled exothermic triplet energy transfer to $^3O_2$ producing $^1O_2$.[20] Similarly, in different studies, Zhang and Castellanoe al.[59,60] decorated blue-emitting InP QDs with 1- and 2-naphthoic acid (NA) and 8-quinolenecarboxylic acid (QCA) to leverage triplet excitons in NCs in concert with surface-anchored molecular acceptors for producing thermally activated delayed photoluminescence (TDPL). The nanohybrids enabled facile bimolecular $^1O_2$ triplet sensitization phosphorescence at 1270 nm.[59,60] Besides, they reported that the QCA was anchored on blue-emitting InP QDs, and its long-lived triplet energy was strategically positioned between the

https://doi.org/10.1021/acsomega.3c03962
ACS Omega 2023, 8, 34328−34353

bright and electron trap states of quantum dots (Figure 16). The nanohybrid was constructed in such a way as to bypass the

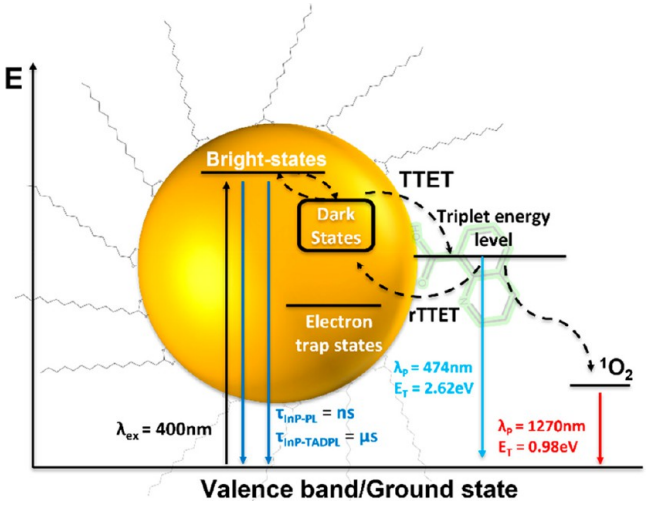

Figure 16. Schematic illustration of InP/QCA nanoconjugates depicting all the relevant photophysical processes and the corresponding energy level diagram. The InP/QCA nanohybrids resulted in a quantitative TTET from the dark states of photoexcited InP QDs to the excited triplet states of surface-bound QCA that subsequently sensitized $^1O_2$ generation. Reproduced with permission from ref 59. Copyright 2022, American Chemical Society.

electron trap in TDPL and repopulate the excitons from excited triplet QCA on the bright state of QDs via rTTET. The QCA-functionalized InP nanohybrids also resulted in a quantitative TTET from photoexcited InP QDs to surface-bound QCA and readily sensitized $^1O_2$ generation, suggesting them as a promising candidate for potential photodynamic therapy.[59]

5.2. Generation of $^1O_2$ by Perovskite QDs. Nowadays, perovskite QDs have emerged as active materials for the sensitization of $^1O_2$ generation involving different mechanisms, e.g., TET, TTET, and energy transfer from defects to dioxygen, thus acting like a versatile sensitizer. Due to the small energy spacing between the dark and bright states (10 meV) of perovskite QDs, the band edge exciton carries mixed features of both dark and bright states irrespective of their ordering. The dark state is treated like the triplet state of the molecular system and plays a deterministic role in the triplet sensitization via the TET process.[40] For instance, Gu et al.[61] studied in detail the generation of $^1O_2$ induced by silica-coated Cs_3PbBr perovskite QDs in the presence of 1,3-diphenylisobenzofuran (DPBF), 3,3′,5,5′-tetramethylbenzidine (TMB), and methyl orange (MO) as the probe molecules. The decrease in the DPBF absorption intensity, turning of colorless TMB into yellowish, and change of orange MO solution into canary suggest that $^1O_2$ is produced by the TET from the QDs to ground state oxygen. To further confirm the formation of $^1O_2$, carotene was introduced as a scavenger with TMB and MO, which significantly inhibited the decomposition of TMB and MO, suggesting that the active substrate produced by the QDs was $^1O_2$. The study demonstrated that the QDs acted as effective photosensitizers to produce $^1O_2$ via TET rather than electron transfer[61] (Figure 17a).

Similarly, Zhang and Xu[62] reported for the first time that metal halide perovskite $MAPbX_3$ (MA: CH_3NH_3, X: Br, I) QDs (having photoluminescence emission at 517 nm and QYs of 0.64) can effectively generate $^1O_2$ with an Φ_{QD} of up to 0.34. The mechanism of $^1O_2$ formation was concluded to be due to TET from QDs to dioxygen. The researchers found that an excited triplet state is formed only when the free charge carriers from different QDs meet and recombine to form a new exciton. If the initial exciton is restrained in the same quantum dot or the photogenerated charge carriers are trapped within the same QDs and have no chance to get out, there will be no formation of a triplet excited state.[62]

Perovskite QDs are known as defect tolerant, enabling them to adopt atoms or ions of appropriate elements into the lattice. Thus, the judicious incorporation of dopant impurities is another way to increase the quantum yields of $^1O_2$. For example, Li et al.[68] incorporated manganese divalent (Mn^{2+}) ions into $CsPbCl_3$ which produced an enhanced amount of $^1O_2$ (Φ_{QDs} = 108%) as compared to 4′-methoxyacetophenone/naphthalene (4′-MAP/N) with known singlet oxygen yield ($\Phi_{4'\text{-MAP/N}}$ = 96%, in cyclohexane). Under irradiation at 355 nm, the QDs transferred its exciton to Mn^{2+} (bulk) in the nanocrystal, which subsequently activated two surface Mn^{2+} defect states followed by nonradiative energy transfers to two surrounding oxygen molecules producing $^1O_2$ (Figure 17b). It was found that with increasing the oxygen amount the luminescence intensities of Mn^{2+} (at 610 nm) and defects (at 950 nm) experienced a continuous decrease, while the phosphorescence of $^1O_2$ (at 1270 nm) exhibited a sharp increase (Figure 17c), substantiating the energy transfer from Mn^{2+} to the ground state of oxygen.[68]

Perovskite QDs also provide a vast platform for dopant impurities and surface-anchored molecular acceptors, which act synergistically to produce an enhanced amount of $^1O_2$. In surface-functionalized nanoconjugates, QDs can transfer energy to surface-anchored molecular sensitizers in a concerted Dexter-like energy transfer or sequential TTET that subsequently sensitizes $^1O_2$ formation. For instance, Luo et al.[66] reported electron-transfer-mediated TET from $CsPbCl_3$ and $CsPbBr_3$ to surface-anchored RhB. It was found that electron transfer from QDs to RhB was also followed by hole transfer. Thus, the RhB sensitized by QDs subsequently interacted with $^3O_2$ generating $^1O_2$.[66]

5.3. Generation of $^1O_2$ by Transition Metal Dichalcogenide QDs. Similar to semiconductor QDs, transition metal dichalcogenides (TMDs) QDs have been reported to generate $^1O_2$ by triplet energy transfer. Under light irradiation, electrons are excited to the CB (excited S_1 state), leaving behind holes on the VB (ground S_0 state). The electrons in the CB are subsequently transferred to the excited T_1 states through ISC where it produces $^1O_2$ via TET to dioxygen.[103] For example, Zhu et al.[102] fabricated blue photoluminescent original MoS_2 QDs (named as O-QDs) with various sulfur contents followed by alkaline etching which created high-density sulfur-vacancy defects to obtain base MoS_2 QDs (named as B-QDs). The increase in defect density was observed to result in decreased energy bandgap and increased active sites, which favored stronger binding affinity toward O_2 (Figure 18d–f). The binding energies of O_2 absorption were found to be enhanced drastically with S defects, thus bringing out a higher content of oxygen on the QDs surface (Figure 18f) and resulting in high quantum yields of the $^1O_2$ generation. The B-QDs demonstrated enhanced generation of ROS as compared to the O-QD system (Figure 18a–c), which was attributed to improved e^-_{CB} and h^+_{VB} pair separation and the reduced energy gap between S_1 and T_1 with a concomitant strengthening binding affinity between QDs and $^3O_2$. It was found that the QDs in S_1 states reacted in two

https://doi.org/10.1021/acsomega.3c03962
ACS Omega 2023, 8, 34328−34353

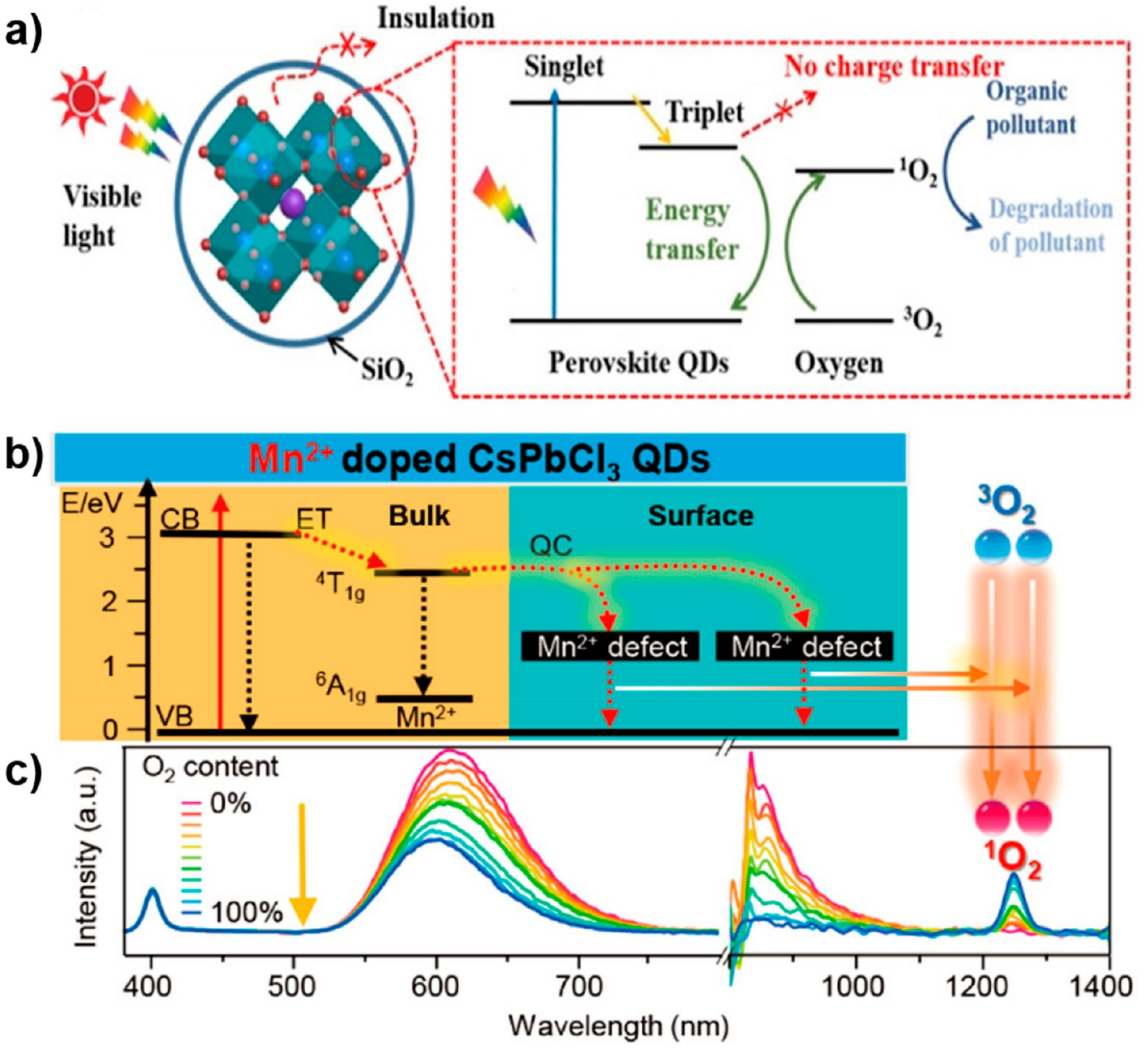

Figure 17. Suggested mechanism for excitonic processes of silica-coated Cs_3PbBr perovskite QDs and the subsequent energy transfer to the oxygen ground state (a). Reproduced with permission from ref 61. Copyright 2019, Wiley-VCH. The proposed mechanism of Mn^{2+}-doped $CsPbCl_3$ for $^1O_2$ generation in which exciton-activated Mn^{2+} transferred its energy to two surface Mn^{2+} defect states subsequently sensitizing $^1O_2$ generation (b). Gradual decline in the luminescence intensities of Mn^{2+} at 610 nm and defect at 950 nm and the concomitant increase in phosphorescence intensity of $^1O_2$ at 1270 with increasing oxygen content (c). Reproduced with permission from ref 68. Copyright 2020, American Chemical Society.

pathways: (a) the QDs interacted with absorbed O_2 to produce $O_2^{-\bullet}$ and $HO^\bullet$ through hydrogen (electron) (type I reaction) and (b) the QDs generated $^1O_2$ through TET to dioxygen (type II reaction)[102] (Figure 18g).

In addition, Zhu et al.[103] reported that MoS_2 with higher surface defects exhibited more effective photodynamic properties to kill cancer cells than those with lower defects at the same concentration, suggesting that this system is a good candidate for PDT. The thickness and size of TMD can also increase the $^1O_2$ and other ROS generation efficiencies. Tian et al.[77] reported the generation of singlet oxygen for MoS_2 QDs by converting $O_2^{-\bullet}$ into $^1O_2$. These QDs exhibited potential antimicrobial properties against *E. coli* and *S. aureus* under environmental conditions as the thickness and size decrease with a trend as shown: MoS_2 QDs > MoS_2 nanosheets > bulk MoS_2. In *in vivo* experiments, the potential antimicrobial activities of QDs showed effective wound healing (Figure 19a−c) under simulated solar light irradiation and exerted protective effects on normal tissues.[77]

Interestingly, TMD also exhibits intrinsic peroxidase-like activity and can decompose H_2O_2 without photoirradiation, producing $^1O_2$ along with other ROS. Li et al.[104] reported the decomposition of H_2O_2 into $^1O_2$ along with other ROS in the presence of MoS_2 QDs. The production capability of ROS depended upon the temperature and concentration of H_2O_2 without artificial control of pH and light irradiation.[104] Similarly, Sun et al.[115] described the generation of $^1O_2$ for WS_2 by the decomposition of H_2O_2 in the presence of sodium hypochlorite. It was found that NaClO oxidized W(IV) of WS_2 to W(VI) which subsequently reacted with H_2O_2 to generate $^1O_2$ and peroxotungstate.[115] TMD has been proposed to couple with other inorganic materials for enhanced $^1O_2$ generation and photodynamic therapy purposes. A composite system of MoS_2 nanosheets loaded with Ag NPs was constructed to form a heterojunction with suppressed electron−hole recombination. Under light irradiation (660 nm), the photogenerated electrons were transferred from MoS_2 to Ag NPs due to the fast transport of silver where they reacted with O_2 to generate $O_2^{-\bullet}$ and $HO^\bullet$, while the photogenerated holes interacted with O_2 to produce

https://doi.org/10.1021/acsomega.3c03962
ACS Omega 2023, 8, 34328−34353

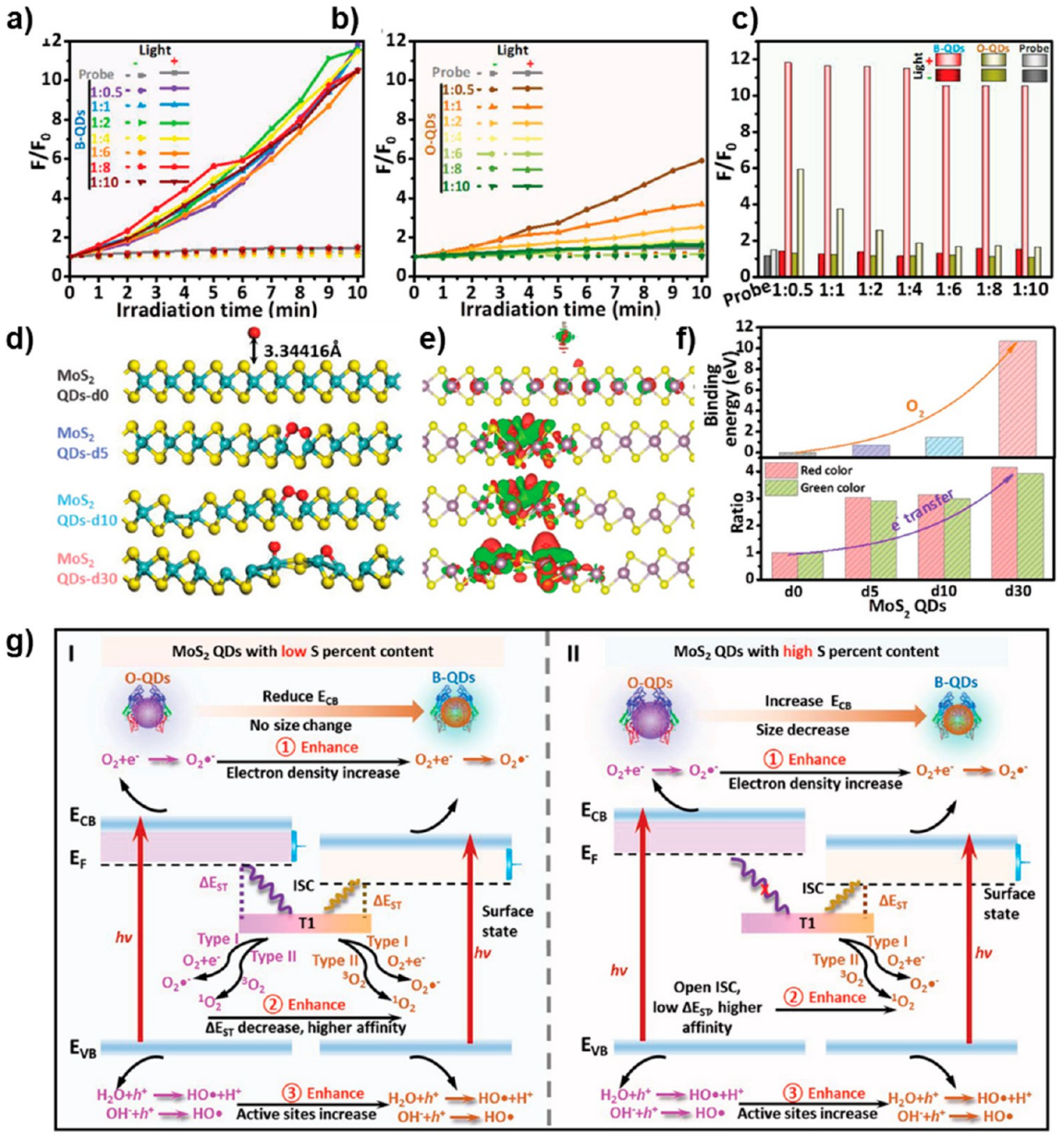

Figure 18. Correlation of ROS generation efficiency of B-QDs (a) and O-QDs (b) as a function of white light irradiation (200−1000 nm) time in the presence of a ROS indicator (H_2DCFHDA) in 1 X PBS (7.4) solution. PL enhancement $[(F - F_0)/F_0]$ of H_2DCFHDA after irradiation in the presence of QDs with various S content, as indicated (c). Optimized geometric structures with increasing degrees of defects (as indicated, d = 0, 5, 10, and 30) of MoS_2-d0, MoS_2-d5, MoS_2-d10, and MoS_2-d30 QDs showing the side view of the Mo−S bond MoS_2: green, yellow, and red spheres stand for the Mo, S, and O atoms, respectively (d). Charge density difference of $^3O_2$ absorbed on the defect binding sites of MoS_2 QDs with various sulfur vacancies; the positive and negative charges are shown in red and green, respectively (e). Correlation between the degrees of defects and binding energy (affinity) of oxygen molecules (upside) and ratios of charge transfer density between $^3O_2$ and defects of QDs (downside) (f). Proposed mechanism of ROS generation by QDs (g). E_{VB}: valence band level. EF: Fermi level. E_{CB}: conduction band level. ISC: intersystem crossing. ΔE_{ST}: the energy gap between singlet excited state (S_1) and triplet excited state (T_1) (① and ③ refer to photocatalysis process, ② refers to photodynamic process). Reproduced with permission from ref 102. Copyright 2022, Wiley-VCH.

$^1O_2$. The Ag/MoS_2 demonstrated enhanced antibacterial efficiency against *S. aureus* (≈98.66%) and *E. coli* (≈99.77%) mainly because of $^1O_2$.[16] The other TMD-based heterojunctions, which have been studied for $^1O_2$-mediated antibacterial purposes, include both MoS_2/Cu[17] and MoS_2/Ag_3PO_4.[18]

6. SUMMARY AND OUTLOOK

Singlet molecular oxygen ($^1O_2$) has been used in a wide array of applications ranging from clinical practices, water purification and wastewater treatment, organic synthesis, and photodegradation to pharmaceutical delivery.[7] Due to the multiple challenges associated with the currently available conventional sensitizers and the need for the next generation sensitizers, this review presents a comprehensive overview of recent designs and developments over the past decade in QDs (i.e., semiconductor QDs, perovskite QDs, and transition metal dichalcogenide QDs) and QD-PS conjugates for the generation of $^1O_2$. We have also described how the chemical composition, optoelectronic properties, and type of surface-anchored molecular acceptor can affect the efficiency of $^1O_2$ production. Traditional sensitizers

https://doi.org/10.1021/acsomega.3c03962
ACS Omega 2023, 8, 34328−34353

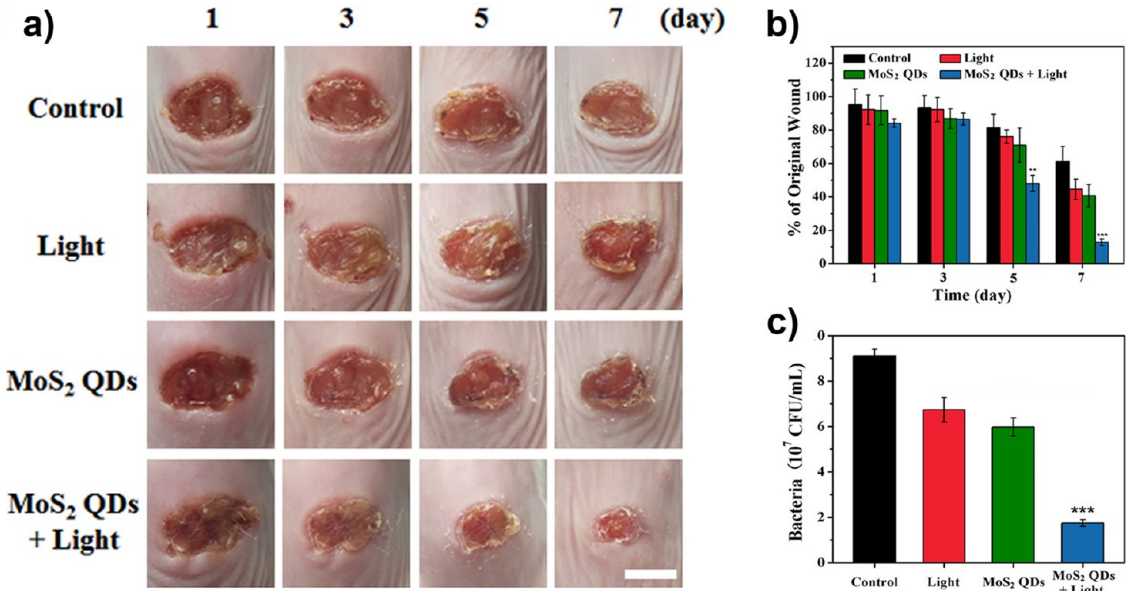

Figure 19. Antibacterial therapeutic performance of the MoS_2 probe in wound-bearing BALB/c mice infected with *S. aureus* under irradiation with white light for 1 h. Representative photographs of *S. aureus* infected wounds of each group harvested after treatment at different times, as indicated (scale bar: 5 mm) (a). Changes in relative wound volumes (b). The number of bacteria from the wound of each group was counted after the seventh day of treatment (c), where $^*p \leq 0.05$; $^{**}p \leq 0.01$; $^{***}p \leq 0.001$. Reproduced with permission from ref 77. Copyright 2019, American Chemical Society.

based on the conjugated π-electronic system have several key challenges, i.e., insolubility in aqueous media, low quantum yields, poor photochemical stability for prolonged time, low extinction coefficients, and large singlet−triplet splitting (hundreds of meV).[5,40,41] For this purpose, QDs have emerged as a highly performant and versatile nanotool to improve the efficiency of $^1O_2$ production. Their unique physicochemical and optoelectronic properties, relying upon a size-dependent quantum confinement effect, composition effect,[5] and mutual alignment of the valence band (VB) and conduction band (CB) of core and shell materials in core−shell heterostructures,[51−54] make them superior over other nanosensitizers. Quantum dots have been reported to show great chemical diversity toward the sensitization of $^1O_2$ generation: they can generate $^1O_2$ either directly by TET to dioxygen[5,61−65] or indirectly by charge transfer[21,63,66,67] to create superoxide radicals which are subsequently converted by QDs to $^1O_2$. Quantum dots provide a vast platform for linking with other organic or metalorganic sensitizers,[20,43,55−60] which transfer excitons to surface-anchored sensitizers through FRET[43,55−57,69−71] or DET/TTET,[58−60] thus subsequently sensitizing $^1O_2$ generation. Quantum dots also offer the opportunity to couple with other inorganic NCs, which is an effective strategy to enhance $^1O_2$ generation due to the improved mobility of interparticle charges and slower electron−hole recombination.[15,21,110,116] Although the photophysical data of $^1O_2$ QYs for individual QDs are not very strong,[5] QDs in combination with other inorganic materials[15,55,110,117] or molecular sensitizers[20,43,55−60] hold great promise to enhance $^1O_2$ production efficiency. Quantum dots can also be surface functionalized with specific ligands, i.e., antibodies or proteins, to achieve active tumor targeting in PDT treatment.[43] Thus, the integration of QDs with other multifunctional modalities improves diagnosis and therapeutic efficacy. Since solid tumor tissues have hypoxic microenvironments and PDT is an oxygen-consuming modality, continuous consumption of O_2 further exacerbates the hypoxic conditions, which limits the efficacy of PDT. QDs can relieve hypoxia by converting H_2O_2 into $^3O_2$ which may be produced in high concentrations by tumor tissues.[104] Based on versatile performance, unique optoelectronics, and physicochemical properties, it is expected that QDs can prove as promising candidates for next-generation sensitizers of $^1O_2$ generation, which will be used for simultaneous diagnosis and PDT modality. However, for clinical applications of QDs in PDT, most of the current research on QDs has been performed for *in vitro* or *in vivo* mice models; therefore, their translation to the human body and more preclinical data are required to understand the pharmacokinetics and pharmacodynamics of bare QDs or QDs coformulated with PS.[53]

AUTHOR INFORMATION

Corresponding Authors

Zahid U. Khan − *Institute of Chemistry, University of Sao Paulo (USP), 05508-000 São Paulo-SP, Brazil;* orcid.org/0000-0003-1529-0832; Email: zahid@iq.usp.br

Paolo Di Mascio − *Institute of Chemistry, University of Sao Paulo (USP), 05508-000 São Paulo-SP, Brazil;* Email: pdmascio@iq.usp.br

Authors

Latif U. Khan − *Institute of Chemistry, University of Sao Paulo (USP), 05508-000 São Paulo-SP, Brazil; Synchrotron-light for Experimental Science and Applications in the Middle East (SESAME), Allan 19252, Jordan;* orcid.org/0000-0002-3535-7099

Hermi F. Brito − *Institute of Chemistry, University of Sao Paulo (USP), 05508-000 São Paulo-SP, Brazil*

Magnus Gidlund − *Institute of Biomedical Sciences-IV, University of Sao Paulo (USP), 05508-000 São Paulo-SP, Brazil;* orcid.org/0000-0003-2047-1136

Oscar L. Malta − *Departamento de Química Fundamental, Universidade Federal de Pernambuco, Recife, PE 50740-560, Brazil*

https://doi.org/10.1021/acsomega.3c03962
ACS Omega 2023, 8, 34328−34353

Complete contact information is available at:
https://pubs.acs.org/10.1021/acsomega.3c03962

Notes

The authors declare no competing financial interest.

■ ACKNOWLEDGMENTS

The authors acknowledge the support of Fundação de Amparo à Pesquisa do Estado de São Paulo (FAPESP) (Z.U.K. no. 2021/00356-6, P.D.M. 2012/12663-1, 2021/08111-2, 2018/21489-1), Conselho Nacional de Desenvolvimento Científico e Tecnológico (CNPq no. 304651/2021-4, 442599/2019-6, 313926/2021-2, P.D.M. 302120/2018-1), The World Academy of Sciences for the advancement of science in developing countries (TWAS) (Z.U.K. no. 190932/2015-5), Brazilian research funding institutions P.D.M. FAPESP CEPID Redoxoma (no. 2013/07937-8), CAPES (Coordenação de Aperfeiçoamento de Pessoal de Nível Superior), PRPUSP (Pro-Reitoria de Pesquisa da Universidade de São Paulo; NAP Redoxoma (P.D.M. no. 2011.1.9352.1.8), the John Simon Guggenheim Memorial Foundation (P.D.M. Fellowship), and XAFS/XRF Beamline of Synchrotron-light for Experimental Science and Applications in the Middle East (SESAME), Jordan.

■ REFERENCES

(1) Bloyet, C.; Sciortino, F.; Matsushita, Y.; Karr, P. A.; Liyanage, A.; Jevasuwan, W.; Fukata, N.; Maji, S.; Hynek, J.; D'Souza, F.; Shrestha, L. K.; Ariga, K.; Yamazaki, T.; Shirahata, N.; Hill, J. P.; Payne, D. T. Photosensitizer Encryption with Aggregation Enhanced Singlet Oxygen Production. *J. Am. Chem. Soc.* **2022**, *144* (24), 10830−10843.

(2) García-Fresnadillo, D. Singlet Oxygen Photosensitizing Materials for Point-of-Use Water Disinfection with Solar Reactors. *ChemPhotoChem.* **2018**, *2* (7), 512−534.

(3) Yang, M.; Zhang, J.; Shabat, D.; Fan, J.; Peng, X. Near-Infrared Chemiluminescent Probe for Real-Time Monitoring Singlet Oxygen in Cells and Mice Model. *ACS Sens.* **2020**, *5* (10), 3158−3164.

(4) Di Mascio, P.; Martinez, G. R.; Miyamoto, S.; Ronsein, G. E.; Medeiros, M. H. G.; Cadet, J. Singlet Molecular Oxygen Reactions with Nucleic Acids, Lipids, and Proteins. *Chem. Rev.* **2019**, *119*, 2043.

(5) Khan, Z. U.; Khan, L. U.; Uchiyama, M. K.; Prado, F. M.; Faria, R. L.; Costa, I. F.; Miyamoto, S.; Araki, K.; Gidlund, M.; Brito, H. F.; Di Mascio, P. Singlet Molecular Oxygen Generation via Unexpected Emission Color-Tunable CdSe/ZnS Nanocrystals for Applications in Photodynamic Therapy. *ACS Appl. Nano Mater.* **2023**, *6* (5), 3767−3780.

(6) Lan, M.; Zhao, S.; Liu, W.; Lee, C. S.; Zhang, W.; Wang, P. Photosensitizers for Photodynamic Therapy. *Adv. Healthc. Mater.* **2019**, *8* (13), 1900132.

(7) Al-Nu'airat, J.; Oluwoye, I.; Zeinali, N.; Altarawneh, M.; Dlugogorski, B. Z. Review of Chemical Reactivity of Singlet Oxygen with Organic Fuels and Contaminants. *Chem. Rec.* **2021**, *21* (2), 315−342.

(8) Calori, I. R.; Bi, H.; Tedesco, A. C. Expanding the Limits of Photodynamic Therapy: The Design of Organelles and Hypoxia-Targeting Nanomaterials for Enhanced Photokilling of Cancer. *ACS Appl. Bio Mater.* **2021**, *4* (1), 195−228.

(9) Kautsky, H. Quenching of luminescence by oxygen,. *Luminescence* **1939**, *35* (35), 216−219.

(10) Seliger, H. A photoelectric method for the measurement of spectra of light sources of rapidly varying intensities,. *Anal. Biochem.* **1960**, *1*, 60−65.

(11) Khan, A. U.; Kasha, M. Red Chemiluminescence of Molecular Oxygen in Aqueous Solution. *J. Chem. Phys.* **1963**, *39* (8), 2105−2106.

(12) Foote, C. S.; Wexler, S. Singlet Oxygen. A Probable Intermediate in Photosensitized Autoxidations. *J. Am. Chem. Soc.* **1964**, *86* (18), 3880−3881.

(13) Karges, J. Clinical Development of Metal Complexes as Photosensitizers for Photodynamic Therapy of Cancer. *Angew. Chemie - Int. Ed.* **2022**, DOI: 10.1002/anie.202112236.

(14) Wang, D.; Zhu, Y.; Wan, X.; Zhang, X.; Zhang, J. Colloidal Semiconductor Nanocrystals for Biological Photodynamic Therapy Applications: Recent Progress and Perspectives. *Prog. Nat. Sci. Mater. Int.* **2020**, *30* (4), 443−455.

(15) Guo, A.; Qin, B.; Qi, Y.; Liu, D.; Ding, M.; Zhang, Y.; Cai, A.; Zhang, F. Singlet Oxygen Mediated Efficient Photocatalytic Degradation of Rhodamine B and Disinfection by ZnO@PDA/Ag-Ag_2O Nanocomposite under LED Light. *J. Alloys Compd.* **2022**, *928*, 167138.

(16) Zhu, M.; Liu, X.; Tan, L.; Cui, Z.; Liang, Y.; Li, Z.; Kwok Yeung, K. W.; Wu, S. Photo-Responsive Chitosan/Ag/MoS_2 for Rapid Bacteria-Killing. *J. Hazard. Mater.* **2020**, *383*, 121122.

(17) Wang, C.; Li, J.; Liu, X.; Cui, Z.; Chen, D. F.; Li, Z.; Liang, Y.; Zhu, S.; Wu, S. The Rapid Photoresponsive Bacteria-Killing of Cu-Doped MoS_2. *Biomater. Sci.* **2020**, *8* (15), 4216−4224.

(18) Zhang, C.; Wang, J.; Chi, R.; Shi, J.; Yang, Y.; Zhang, X. Reduced Graphene Oxide Loaded with MoS_2 and Ag_3PO_4 Nanoparticles/PVA Interpenetrating Hydrogels for Improved Mechanical and Antibacterial Properties. *Mater. Des.* **2019**, *183*, 108166.

(19) Jiang, Y.; López-Arteaga, R.; Weiss, E. A. Quantum Dots Photocatalyze Intermolecular [2 + 2] Cycloadditions of Aromatic Alkenes Adsorbed to Their Surfaces via van Der Waals Interactions. *J. Am. Chem. Soc.* **2022**, *144* (9), 3782−3786.

(20) Mongin, C.; Garakyaraghi, S.; Razgoniaeva, N.; Zamkov, M.; Castellano, F. N. Direct Observation of Triplet Energy Transfer from Semiconductor Nanocrystals. *Science (80-).* **2016**, *351* (6271), 369−372.

(21) Zhou, N.; Zhu, H.; Li, S.; Yang, J.; Zhao, T.; Li, Y.; Xu, Q. H. Au Nanorod/ZnO Core-Shell Nanoparticles as Nano-Photosensitizers for Near-Infrared Light-Induced Singlet Oxygen Generation. *J. Phys. Chem. C* **2018**, *122* (14), 7824−7830.

(22) Steinbeck, M. J.; Khan, A. U.; Karnovsky, M. J. Intracellular Singlet Oxygen Generation by Phagocytosing Neutrophils in Response to Particles Coated with a Chemical Trap. *J. Biol. Chem.* **1992**, *267* (19), 13425−13433.

(23) Berra, C. M.; Menck, C. F. M.; Di Mascio, P. Estresse oxidativo, lesões no genoma e processos de sinalização no controle do ciclo celular. *Quim. Nova* **2006**, *29* (6), 1340−1344.

(24) Yagura, T.; Schuch, A. P.; Garcia, C. C. M.; Rocha, C. R. R.; Moreno, N. C.; Angeli, J. P. F.; Mendes, D.; Severino, D.; Bianchini Sanchez, A.; Di Mascio, P.; de Medeiros, M. H. G.; Menck, C. F. M. Direct Participation of DNA in the Formation of Singlet Oxygen and Base Damage under UVA Irradiation. *Free Radic. Biol. Med.* **2017**, *108*, 86−93.

(25) Cadet, J.; Davies, K. J. A.; Medeiros, M. H. G; Di Mascio, P.; Wagner, J. R. Formation and Repair of Oxidatively Generated Damage in Cellular DNA. *Free Radic. Biol. Med.* **2017**, *107*, 13−34.

(26) Stanley, C. P.; Maghzal, G. J.; Ayer, A.; Talib, J.; Giltrap, A. M.; Shengule, S.; Wolhuter, K.; Wang, Y.; Chadha, P.; Suarna, C.; Prysyazhna, O.; Scotcher, J.; Dunn, L. L.; Prado, F. M.; Nguyen, N.; Odiba, J. O.; Baell, J. B.; Stasch, J. P.; Yamamoto, Y.; Di Mascio, P.; Eaton, P.; Payne, R. J.; Stocker, R. Singlet Molecular Oxygen Regulates Vascular Tone and Blood Pressure in Inflammation. *Nature* **2019**, *566* (7745), 548−552.

(27) Adam, W.; Kazakov, D. V.; Kazakov, V. P. Singlet-Oxygen Chemiluminescence in Peroxide Reactions. *Chem. Rev.* **2005**, *105* (9), 3371−3387.

(28) Kanofsky, J. R.; Axelrod, B. Singlet Oxygen Production by Soybean Lipoxygenase Isozymes. *J. Biol. Chem.* **1986**, *261* (3), 1099−1104.

(29) Klebanoff, S. J. Myeloperoxidase: Friend and Foe. *J. Leukoc. Biol.* **2005**, *77* (5), 598−625.

(30) Muñoz, F.; Mvula, E.; Braslavsky, S. E.; Von Sonntag, C. Singlet Dioxygen Formation in Ozone Reactions in Aqueous Solution. *J. Chem. Soc. Perkin Trans. 2* **2001**, No. 7, 1109−1116.

(31) Uemi, M.; Ronsein, G. E.; Miyamoto, S.; Medeiros, M. H. G.; Di Mascio, P. Generation of Cholesterol Carboxyaldehyde by the Reaction

of Singlet Molecular Oxygen [O_2 ($^1\Delta_g$)] as Well as Ozone with Cholesterol. *Chem. Res. Toxicol.* **2009**, *22* (5), 875−884.
(32) Di Mascio, P.; Bechara, E. J.H.; Medeiros, M. H.G.; Briviba, K.; Sies, H. Singlet molecular oxygen production in the reaction of peroxynitrite with hydrogen peroxide. *Hydrogen Peroxide* **1994**, *355*, 287−289.
(33) Miyamoto, S.; Ronsein, G. E.; Corrêa, T. C.; Martinez, G. R.; Medeiros, M. H. G.; Di Mascio, P. Direct Evidence of Singlet Molecular Oxygen Generation from Peroxynitrate, a Decomposition Product of Peroxynitrite. *Dalt. Trans.* **2009**, No. 29, 5720−5729.
(34) Miyamoto, S.; Martinez, G. R.; Martins, A. P. B.; Medeiros, M. H. G.; Di Mascio, P. Direct Evidence of Singlet Molecular Oxygen [O_2 ($^1\Delta_g$)] Production in the Reaction of Linoleic Acid Hydroperoxide with Peroxynitrite. *J. Am. Chem. Soc.* **2003**, *125* (15), 4510−4517.
(35) Bastos, E. L.; Farahani, P.; Bechara, E. J. H.; Baader, W. J. Four-Membered Cyclic Peroxides: Carriers of Chemical Energy. *J. Phys. Org. Chem.* **2017**, *30* (9), 3725.
(36) Mano, C. M.; Prado, F. M.; Massari, J.; Ronsein, G. E.; Martinez, G. R.; Miyamoto, S.; Cadet, J.; Sies, H.; Medeiros, M. H. G.; Bechara, E. J. H.; Di Mascio, P. Excited Singlet Molecular O_2 ($^1\delta_g$) Is Generated Enzymatically From Excited Carbonyls In The Dark. *Sci. Rep.* **2014**, *4*, 1−10.
(37) Baptista, M. S.; Cadet, J.; Di Mascio, P.; Ghogare, A. A.; Greer, A.; Hamblin, M. R.; Lorente, C.; Nunez, S. C.; Ribeiro, M. S.; Thomas, A. H.; Vignoni, M.; Yoshimura, T. M. Type I and Type II Photosensitized Oxidation Reactions: Guidelines and Mechanistic Pathways. *Photochem. Photobiol.* **2017**, *93* (4), 912−919.
(38) Aubry, J. M.; Cazin, B. Chemical Sources of Singlet Oxygen. 2. Quantitative Generation of Singlet Oxygen from Hydrogen Peroxide Disproportionation Catalyzed by Molybdate Ions. *Inorg. Chem.* **1988**, *27* (12), 2013−2014.
(39) Corey, E. J.; Taylor, W. C. A Study of the Peroxidation of Organic Compounds by Externally Generated Singlet Oxygen Molecules. *J. Am. Chem. Soc.* **1964**, *86* (18), 3881−3882.
(40) Mondal, N.; De, A.; Seth, S.; Ahmed, T.; Das, S.; Paul, S.; Gautam, R. K.; Samanta, A. Dark Excitons of the Perovskites and Sensitization of Molecular Triplets. *ACS Energy Lett.* **2021**, *6* (2), 588−597.
(41) Han, Y.; He, S.; Wu, K. Molecular Triplet Sensitization and Photon Upconversion Using Colloidal Semiconductor Nanocrystals. *ACS Energy Lett.* **2021**, *6* (9), 3151−3166.
(42) Kargozar, S.; Hoseini, S. J.; Milan, P. B.; Hooshmand, S.; Kim, H. W.; Mozafari, M. Quantum Dots: A Review from Concept to Clinic. *Biotechnol. J.* **2020**, *15* (12), 2000117.
(43) Shen, Y.; Sun, Y.; Yan, R.; Chen, E.; Wang, H.; Ye, D.; Xu, J. J.; Chen, H. Y. Rational Engineering of Semiconductor QDs Enabling Remarkable $^1O_2$ Production for Tumor-Targeted Photodynamic Therapy. *Biomaterials* **2017**, *148*, 31−40.
(44) Torimoto, T.; Adachi, T.; Okazaki, K.; Sakuraoka, M.; Shibayama, T.; Ohtani, B.; Kudo, A.; Kuwabata, S. Facile Synthesis of ZnS-AgInS2 Solid Solution Nanoparticles for a Color-Adjustable Luminophore. *J. Am. Chem. Soc.* **2007**, *129* (41), 12388−12389.
(45) Yang, X.; Tang, Y.; Tan, S. T.; Bosman, M.; Dong, Z.; Leck, K. S.; Ji, Y.; Demir, H. V.; Sun, X. W. Facile Synthesis of Luminescent $AgInS_2$-ZnS Solid Solution Nanorods. *Small* **2013**, *9* (16), 2689−2695.
(46) Kagan, C. R.; Bassett, L. C.; Murray, C. B.; Thompson, S. M. Colloidal Quantum Dots as Platforms for Quantum Information Science. *Chem. Rev.* **2021**, *121* (5), 3186−3233.
(47) Nagelj, N.; Brumberg, A.; Peifer, S.; Schaller, R. D.; Olshansky, J. H. Compositionally Tuning Electron Transfer from Photoexcited Core/Shell Quantum Dots via Cation Exchange. *J. Phys. Chem. Lett.* **2022**, *13* (14), 3209−3216.
(48) Wang, Z.; Zhang, X.; Xin, W.; Yao, D.; Liu, Y.; Zhang, L.; Liu, W.; Zhang, W.; Zheng, W.; Yang, B.; Zhang, H. Facile Synthesis of Cu-In-S/ZnS Core/Shell Quantum Dots in 1-Dodecanethiol for Efficient Light-Emitting Diodes with an External Quantum Efficiency of 7.8%. *Chem. Mater.* **2018**, *30* (24), 8939−8947.
(49) Jun, S.; Jang, E. Interfused Semiconductor Nanocrystals: Brilliant Blue Photoluminescence and Electroluminescence. *Chem. Commun.* **2005**, *1* (36), 4616−4618.
(50) Efros, A. L.; Brus, L. E. Nanocrystal Quantum Dots: From Discovery to Modern Development. *ACS Nano* **2021**, *15* (4), 6192−6210.
(51) Selopal, G. S.; Zhao, H.; Wang, Z. M.; Rosei, F. Core/Shell Quantum Dots Solar Cells. *Adv. Funct. Mater.* **2020**, *30* (13), 1908762.
(52) Yang, G.; Kazes, M.; Raanan, D.; Oron, D. Bright Near-Infrared to Visible Upconversion Double Quantum Dots Based on a Type-II/Type-I Heterostructure. *ACS Photonics* **2021**, *8* (7), 1909−1916.
(53) Uprety, B.; Abrahamse, H. Semiconductor Quantum Dots for Photodynamic Therapy: Recent Advances. *Front. Chem.* **2022**, *10* (8), 1−17.
(54) Sahu, A.; Kumar, D. Core-Shell Quantum Dots: A Review on Classification, Materials, Application, and Theoretical Modeling. *J. Alloys Compd.* **2022**, *924*, 166508.
(55) Li, Y.; Li, Y.; Bai, Y.; Wang, R.; Lin, L.; Sun, Y. Semiconductor ZnO Based Photosensitizer Core-Shell Upconversion Nanoparticle Heterojunction for Photodynamic Therapy. *RSC Adv.* **2020**, *10* (63), 38416−38423.
(56) Tsolekile, N.; Parani, S.; de Macedo, E. F.; Lebepe, T. C.; Maluleke, R.; Ncapayi, V.; Matoetoe, M. C.; Songca, S. P.; Conceição, K.; Tada, D. B.; Oluwafemi, O. S. Photodynamic Therapy and Antibacterial Activities of a Novel Synthesized Quaternary Zn-Cu-In-S/ZnS QDs-MTHPP Porphyrin Conjugate. *Int. J. Nanomedicine* **2022**, *17*, 5315−5325.
(57) Sewid, F. A.; Annas, K. I.; Dubavik, A.; Veniaminov, A. V.; Maslov, V. G.; Orlova, A. O. Chitosan Nanocomposites with CdSe/ZnS Quantum Dots and Porphyrin. *RSC Adv.* **2021**, *12* (2), 899−906.
(58) Mongin, C.; Moroz, P.; Zamkov, M.; Castellano, F. N. Thermally Activated Delayed Photoluminescence from Pyrenyl-Functionalized CdSe Quantum Dots. *Nat. Chem.* **2018**, *10* (2), 225−230.
(59) Zhang, X.; Castellano, F. N. Thermally Activated Bright-State Delayed Blue Photoluminescence from InP Quantum Dots. *J. Phys. Chem. Lett.* **2022**, *13* (16), 3706−3711.
(60) Zhang, X.; Hudson, M. H.; Castellano, F. N. Engineering Long-Lived Blue Photoluminescence from InP Quantum Dots Using Isomers of Naphthoic Acid. *J. Am. Chem. Soc.* **2022**, *144* (8), 3527−3534.
(61) Gu, K.; Wang, Y.; Shen, J.; Zhu, J.; Zhu, Y.; Li, C. Effective Singlet Oxygen Generation in Silica-Coated $CsPbBr_3$ Quantum Dots through Energy Transfer for Photocatalysis. *ChemSusChem* **2020**, *13* (4), 682−687.
(62) Zhang, X. F.; Xu, B. Organo Metal Halide Perovskites Effectively Photosensitize the Production of Singlet Oxygen ($^1\Delta_g$). *Chem. Commun.* **2019**, *55* (87), 13100−13103.
(63) Bailón-Ruiz, S.; Perales-Pérez, O. J. Generation of Singlet Oxygen by Water-Stable CdSe(S) and ZnSe(S) Quantum Dots. *Appl. Mater. Today* **2017**, *9*, 161−166.
(64) Li, Y.; Zhang, P.; Tang, W.; Mchugh, K. J.; Kershaw, S. V.; Jiao, M.; Huang, X.; Kalytchuk, S.; Perkinson, C. F.; Yue, S.; Qiao, Y.; Zhu, L.; Jing, L.; Gao, M.; Han, B. Bright, Magnetic NIR-II Quantum Dot Probe for Sensitive Dual-Modality Imaging and Intensive Combination Therapy of Cancer. *ACS Nano* **2022**, *16*, 8076.
(65) He, T.; Qiu, X.; Li, J.; Pang, G.; Wu, Z.; Cheng, J.; Zhou, Z.; Hao, J.; Liu, H.; Ni, Y.; Li, L.; Lin, X.; Hu, W.; Wang, K.; Chen, R. Water-Soluble Chiral CdSe/CdS Dot/Rod Nanocrystals for Two-Photon Fluorescence Lifetime Imaging and Photodynamic Therapy. *Nanoscale* **2019**, *11* (32), 15245−15252.
(66) Luo, X.; Liang, G.; Han, Y.; Li, Y.; Ding, T.; He, S.; Liu, X.; Wu, K. Triplet Energy Transfer from Perovskite Nanocrystals Mediated by Electron Transfer. *J. Am. Chem. Soc.* **2020**, *142* (25), 11270−11278.
(67) Wang, M.; Nian, L.; Cheng, Y.; Yuan, B.; Cheng, S.; Cao, C. Encapsulation of Colloidal Semiconductor Quantum Dots into Metal-Organic Frameworks for Enhanced Antibacterial Activity through Interfacial Electron Transfer. *Chem. Eng. J.* **2021**, *426* (5), 130832.
(68) Li, D.; Li, X.; Zhao, T.; Liu, H.; Jiang, S.; Zhang, Q.; Ågren, H.; Chen, G. Ultraefficient Singlet Oxygen Generation from Manganese-

https://doi.org/10.1021/acsomega.3c03962
ACS Omega 2023, 8, 34328−34353

Doped Cesium Lead Chloride Perovskite Quantum Dots. *ACS Nano* **2020**, *14* (10), 12596−12604.
(69) Sewid, F. A.; Visheratina, A. K.; Dubavik, A.; Veniaminov, A. V.; Maslov, V. G.; Orlova, A. O. Chlorin e6-CdSe/ZnS Quantum Dots Nanocomposites as Efficient Singlet Oxygen Generator. *Opt. Spectrosc.* **2019**, *127* (6), 1104−1109.
(70) Drozdek, S.; Szeremeta, J.; Lamch, L.; Nyk, M.; Samoc, M.; Wilk, K. A. Two-Photon Induced Fluorescence Energy Transfer in Polymeric Nanocapsules Containing $CdSe_xS_{1-x}$/ZnS Core/Shell Quantum Dots and Zinc(II) Phthalocyanine. *J. Phys. Chem. C* **2016**, *120* (28), 15460−15470.
(71) Monte, A. F. G.; Azevedo, G.; Reis, A. F. Spatial Energy Transfer with Observation of Bimolecular Singlet Oxygen Emission Using Quantum Dots as Donors and Zinc-Phthalocyanine as Acceptors. *Luminescence* **2020**, *35* (5), 667−672.
(72) Pu, Y.; Cai, F.; Wang, D.; Wang, J. X.; Chen, J. F. Colloidal Synthesis of Semiconductor Quantum Dots toward Large-Scale Production: A Review. *Ind. Eng. Chem. Res.* **2018**, *57* (6), 1790−1802.
(73) Dhamo, L.; Wegner, K. D.; Würth, C.; Häusler, I.; Hodoroaba, V. D.; Resch-Genger, U. Assessing the Influence of Microwave-Assisted Synthesis Parameters and Stabilizing Ligands on the Optical Properties of AIS/ZnS Quantum Dots. *Sci. Rep.* **2022**, *12* (1), 1−11.
(74) Castano, A. P.; Demidova, T. N.; Hamblin, M. R. Mechanisms in Photodynamic Therapy: Part One - Photosensitizers, Photochemistry and Cellular Localization. *Photodiagnosis Photodyn. Ther.* **2004**, *1* (4), 279−293.
(75) Öztürk, D.; Ömeroglu, I.; Durmus, M. Quantum Dots in Photodynamic Therapy. *Nanomaterials for Photodynamic Therapy* **2023**, 401−439.
(76) Tyrrell, R. M. Role for Singlet Oxygen in Biological Effects of Ultraviolet A Radiation. *Methods Enzymol.* **2000**, *319* (1977), 290−296.
(77) Tian, X.; Sun, Y.; Fan, S.; Boudreau, M. D.; Chen, C.; Ge, C.; Yin, J. J. Photogenerated Charge Carriers in Molybdenum Disulfide Quantum Dots with Enhanced Antibacterial Activity. *ACS Appl. Mater. Interfaces* **2019**, *11* (5), 4858−4866.
(78) De Biologia, R. C.; Riberio, D. T.; Nigro, R. G.; Di Mascio, P.; Menck, C. F. M. Singlet Oxygen Induced Mutation Spectrum in Mammalian Cells. *Nucleic Acids Res.* **1992**, *20* (16), 4319−4323.
(79) Ravanat, J. L.; Martinez, G. R.; Medeiros, M. H. G.; Di Mascio, P.; Cadet, J. Singlet Oxygen Oxidation of 2′-Deoxyguanosine. Formation and Mechanistic Insights. *Tetrahedron* **2006**, *62* (46), 10709−10715.
(80) Pinto, E.; Catalani, L. H.; Lopes, N. P.; Di Mascio, P.; Colepicolo, P. Peridinin as the Major Biological Carotenoid Quencher of Singlet Oxygen in Marine Algae Gonyaulax Polyedra. *Biochem. Biophys. Res. Commun.* **2000**, *268* (2), 496−500.
(81) Yang, D.-C.; Wang, S.; Weng, X.-L.; Zhang, H.-X.; Liu, J.-Y.; Lin, Z. Singlet Oxygen-Responsive Polymeric Nanomedicine for Light-Controlled Drug Release and Image-Guided Photodynamic-Chemo Combination Therapy. *ACS Appl. Mater. & Interfaces* **2021**, *13* (29), 33905−33914.
(82) Liu, J.; Yang, G.; Zhu, W.; Dong, Z.; Yang, Y.; Chao, Y.; Liu, Z. Light-Controlled Drug Release from Singlet-Oxygen Sensitive Nanoscale Coordination Polymers Enabling Cancer Combination Therapy. *Biomaterials* **2017**, *146*, 40−48.
(83) Mo, Y.; Cheng, M. H. Y.; D'Elia, A.; Doran, K.; Ding, L.; Chen, J.; Cullis, P. R.; Zheng, G. Light-Activated SiRNA Endosomal Release (LASER) by Porphyrin Lipid Nanoparticles. *ACS Nano* **2023**, *17* (5), 4688−4703.
(84) Aerssens, D.; Cadoni, E.; Tack, L.; Madder, A. A Photosensitized Singlet Oxygen ($^1O_2$) Toolbox for Bio-Organic Applications: Tailoring $^1O_2$ Generation for DNA and Protein Labelling, Targeting and Biosensing. *Molecules* **2022**, *27* (3), 778.
(85) Choi, H.; Kim, M.; Jang, J.; Hong, S. Visible-Light-Induced Cysteine-Specific Bioconjugation: Biocompatible Thiol-Ene Click Chemistry. *Angew. Chemie - Int. Ed.* **2020**, *59* (50), 22514−22522.
(86) Vera, C. C.; Borsarelli, C. D. Photo-Induced Protein Modifications: A Range of Biological Consequences and Applications. *Biophys. Rev.* **2023**, DOI: 10.1007/s12551-023-01081-6.
(87) Van Hoorick, J.; Tytgat, L.; Dobos, A.; Ottevaere, H.; Van Erps, J.; Thienpont, H.; Ovsianikov, A.; Dubruel, P.; Van Vlierberghe, S. (Photo-)Crosslinkable Gelatin Derivatives for Biofabrication Applications. *Acta Biomater.* **2019**, *97*, 46−73.
(88) Abbate, V.; Kong, X.; Bansal, S. S. Photocrosslinked Bovine Serum Albumin Hydrogels with Partial Retention of Esterase Activity. *Enzyme Microb. Technol.* **2012**, *50* (2), 130−136.
(89) Khan, Z. U.; Uchiyama, M. K.; Khan, L. U.; Ramos-Sanchez, E. M.; Reis, L. C.; Nakamura, M.; Goto, H.; De Souza, A. O.; Araki, K.; Brito, H. F.; Gidlund, M. Orange-Emitting ZnSe:Mn2+ Quantum Dots as Nanoprobes for Macrophages. *ACS Appl. Nano Mater.* **2020**, *3* (10), 10399−10410.
(90) Khan, Z. U.; Uchiyama, M. K.; Khan, L. U.; Araki, K.; Goto, H.; Felinto, M. C. F. C.; De Souza, A. O.; De Brito, H. F.; Gidlund, M. Wide Visible-Range Activatable Fluorescence ZnSe:Eu^{3+}/Mn^{2+}@ZnS Quantum Dots: Local Atomic Structure Order and Application as a Nanoprobe for Bioimaging. *J. Mater. Chem. B* **2022**, *10* (2), 247−261.
(91) Khan, L. U.; Khan, Z. U.; Blois, L.; Tabassam, L.; Brito, H. F.; Figueroa, S. J. A. Strategy to Probe the Local Atomic Structure of Luminescent Rare Earth Complexes by X-Ray Absorption Near-Edge Spectroscopy Simulation Using a Machine Learning-Based PyFitIt Approach. *Inorg. Chem.* **2023**, *62* (6), 2738−2750.
(92) Hashemkhani, M.; Loizidou, M.; MacRobert, A. J.; Yagci Acar, H. One-Step Aqueous Synthesis of Anionic and Cationic $AgInS_2$ Quantum Dots and Their Utility in Improving the Efficacy of ALA-Based Photodynamic Therapy. *Inorg. Chem.* **2022**, *61* (6), 2846−2863.
(93) Huang, H.; Lovell, J. F. Advanced Functional Nanomaterials for Theranostics. *Adv. Funct. Mater.* **2017**, *27* (2), 1603524.
(94) Gholizadeh, E. M.; Prasad, S. K. K.; Teh, Z. L.; Ishwara, T.; Norman, S.; Petty, A. J.; Cole, J. H.; Cheong, S.; Tilley, R. D.; Anthony, J. E.; Huang, S.; Schmidt, T. W. Photochemical Upconversion of Near-Infrared Light from below the Silicon Bandgap. *Nat. Photonics* **2020**, *14* (9), 585−590.
(95) Ekimov, A. I.; Efros, A. L.; Onushchenko, A. A. Quantum Size Effect in Semiconductor Microcrystals. *Solid State Commun.* **1985**, *56* (11), 921−924.
(96) Brus, L. E. Electron-Electron and Electron-Hole Interactions in Small Semiconductor Crystallites: The Size Dependence of the Lowest Excited Electronic State. *J. Chem. Phys.* **1984**, *80* (9), 4403−4409.
(97) Huang, Z.; Xia, P.; Megerdich, N.; Fishman, D. A.; Vullev, V. I.; Tang, M. L. ZnS Shells Enhance Triplet Energy Transfer from CdSe Nanocrystals for Photon Upconversion. *ACS Photonics* **2018**, *5* (8), 3089−3096.
(98) Jin, T.; He, S.; Zhu, Y.; Egap, E.; Lian, T. Bright State Sensitized Triplet Energy Transfer from Quantum Dot to Molecular Acceptor Revealed by Temperature Dependent Energy Transfer Dynamics. *Nano Lett.* **2022**, *22* (10), 3897−3903.
(99) Gray, V.; Zhang, Z.; Dowland, S.; Allardice, J. R.; Alvertis, A. M.; Xiao, J.; Greenham, N. C.; Anthony, J. E.; Rao, A. Thiol-Anchored TIPS-Tetracene Ligands with Quantitative Triplet Energy Transfer to PbS Quantum Dots and Improved Thermal Stability. *J. Phys. Chem. Lett.* **2020**, *11* (17), 7239−7244.
(100) Irgen-Gioro, S.; Yang, M.; Padgaonkar, S.; Chang, W. J.; Zhang, Z.; Nagasing, B.; Jiang, Y.; Weiss, E. A. Charge and Energy Transfer in the Context of Colloidal Nanocrystals. *Chem. Phys. Rev.* **2020**, *1* (1), 011305.
(101) Nguyen, V. H.; Nguyen, T. P.; Le, T. H.; Vo, D. V. N.; Nguyen, D. L. T.; Trinh, Q. T.; Kim, I. T.; Le, Q. Van. Recent Advances in Two-Dimensional Transition Metal Dichalcogenides as Photoelectrocatalyst for Hydrogen Evolution Reaction. *J. Chem. Technol. Biotechnol.* **2020**, *95* (10), 2597−2607.
(102) Zhu, H.; et al. Defect-Rich Molybdenum Sulfide quantum dots for amplified photoluminescence and photonics-driven reactive oxygen species generation. *Adv. Mater.* **2022**, *34* (31), 2200004.
(103) Ding, X.; Peng, F.; Zhou, J.; Gong, W.; Slaven, G.; Loh, K. P.; Lim, C. T.; Leong, D. T. Defect Engineered Bioactive Transition Metals Dichalcogenides Quantum Dots. *Nat. Commun.* **2019**, DOI: 10.1038/s41467-018-07835-1.

(104) Li, Q.; Hu, B.; Yang, Q.; Cai, X.; Nie, M.; Jin, Y.; Zhou, L.; Xu, Y.; Pan, Q.; Fang, L. Interaction Mechanism between Multi-Layered MoS_2 and H_2O_2 for Self-Generation of Reactive Oxygen Species. *Environ. Res.* **2020**, *191* (9), 110227.
(105) Chowdhury, T.; Sadler, E. C.; Kempa, T. J. Progress and Prospects in Transition-Metal Dichalcogenide Research beyond 2D. *Chem. Rev.* **2020**, *120* (22), 12563−12591.
(106) Wang, L.; Xu, D.; Jiang, L.; Gao, J.; Tang, Z.; Xu, Y.; Chen, X.; Zhang, H. Transition Metal Dichalcogenides for Sensing and Oncotherapy: Status, Challenges, and Perspective. *Adv. Funct. Mater.* **2021**, *31* (5), 2004408.
(107) Araki, K.; Silva, C. A.; Toma, H. E.; Catalani, L. H.; Medeiros, M. H. G.; Di Mascio, P. Zinc Tetraruthenated Porphyrin Binding and Photoinduced Oxidation of Calf-Thymus DNA. *J. Inorg. Biochem.* **2000**, *78* (4), 269−273.
(108) George, B. P.; Chota, A.; Sarbadhikary, P.; Abrahamse, H. Fundamentals and Applications of Metal Nanoparticle- Enhanced Singlet Oxygen Generation for Improved Cancer Photodynamic Therapy. *Front. Chem.* **2022**, *10* (July), 1−14.
(109) Beltrán-García, M. J.; Prado, F. M.; Oliveira, M. S.; Ortiz-Mendoza, D.; Scalfo, A. C.; Pessoa, A.; Medeiros, M. H. G.; White, J. F.; Di Mascio, P. Singlet Molecular Oxygen Generation by Light-Activated DHN-Melanin of the Fungal Pathogen Mycosphaerella Fijiensis in Black Sigatoka Disease of Bananas. *PLoS One* **2014**, *9* (3), e91616.
(110) Huo, P.; Guan, J.; Zhou, M.; Ma, C.; Liu, X.; Yan, Y.; Yuan, S. Carbon Quantum Dots Modified CdSe Loaded Reduced Graphene Oxide for Enhancing Photocatalytic Activity. *J. Ind. Eng. Chem.* **2017**, *50*, 147−154.
(111) Li, B.; Lin, L.; Lin, H.; Wilson, B. C. Photosensitized Singlet Oxygen Generation and Detection: Recent Advances and Future Perspectives in Cancer Photodynamic Therapy. *J. Biophotonics* **2016**, *9* (11−12), 1314−1325.
(112) Vanorman, Z. A.; Bieber, A. S.; Wieghold, S.; Nienhaus, L. Green-to-Blue Triplet Fusion Upconversion Sensitized by Anisotropic CdSe Nanoplatelets. *Chem. Mater.* **2020**, *32* (11), 4734−4742.
(113) Dai, X.; Du, T.; Han, K. Engineering Nanoparticles for Optimized Photodynamic Therapy. *ACS Biomaterials Science and Engineering.* **2019**, *5*, 6342−6354.
(114) Jiang, Y.; Weiss, E. A. Colloidal Quantum Dots as Photocatalysts for Triplet Excited State Reactions of Organic Molecules. *J. Am. Chem. Soc.* **2020**, *142* (36), 15219−15229.
(115) Sun, T.; Su, Y.; Sun, M.; Lv, Y. Homologous Chemiluminescence Resonance Energy Transfer on the Interface of WS_2 Quantum Dots for Monitoring Photocatalytic H2O2 Evaluation. *Microchem. J.* **2021**, *168* (3), 106344.
(116) Li, J.; Liu, K.; Xue, J.; Xue, G.; Sheng, X.; Wang, H.; Huo, P.; Yan, Y. CQDs Preluded Carbon-Incorporated 3D Burger-like Hybrid ZnO Enhanced Visible-Light-Driven Photocatalytic Activity and Mechanism Implication. *J. Catal.* **2019**, *369*, 450−461.
(117) Wang, W. N.; Huang, C. X.; Zhang, C. Y.; Zhao, M. L.; Zhang, J.; Chen, H. J.; Zha, Z. B.; Zhao, T.; Qian, H. S. Controlled Synthesis of Upconverting Nanoparticles/$Zn_xCd_{1-X}S$ Yolk-Shell Nanoparticles for Efficient Photocatalysis Driven by NIR Light. *Appl. Catal. B Environ.* **2018**, *224* (11), 854−862.
(118) Zhu, H.; Zan, W.; Chen, W.; Jiang, W.; Ding, X.; Li, B. L.; Mu, Y.; Wang, L.; Garaj, S.; Leong, D. T. Defect-Rich Molybdenum Sulfide Quantum Dots for Amplified Photoluminescence and Photonics-Driven Reactive Oxygen Species Generation. *Adv. Mater.* **2022**, *34* (31), 12200004.
(119) Dubose, J. T.; Kamat, P. V. Directing Energy Transfer in Halide Perovskite-Chromophore Hybrid Assemblies. *J. Am. Chem. Soc.* **2021**, *143* (45), 19214−19223.
(120) DuBose, J. T.; Kamat, P. V. Energy Versus Electron Transfer: Managing Excited-State Interactions in Perovskite Nanocrystal-Molecular Hybrids. *Chem. Rev.* **2022**, *122* (15), 12475−12494.
(121) Wang, T.; Wang, X.; Yang, R.; Li, C. Recent Advances in Ternary Organic Solar Cells Based on Förster Resonance Energy Transfer. *Sol. RRL* **2021**, *5* (12), 2100496.
(122) Bai, S.; Zhang, P.; Beratan, D. N. Predicting Dexter Energy Transfer Interactions from Molecular Orbital Overlaps. *J. Phys. Chem. C* **2020**, *124* (35), 18956−18960.
(123) Zhu, H.; Yang, Y.; Wu, K.; Lian, T. Charge Transfer Dynamics from Photoexcited Semiconductor Quantum Dots. *Annu. Rev. Phys. Chem.* **2016**, *67*, 259−281.
(124) Uprety, B.; Abrahamse, H. Semiconductor Quantum Dots for Photodynamic Therapy: Recent Advances. *Front. Chem.* **2022**, *10*, 15736−15737.
(125) Yonemoto, D. T.; Papa, C. M.; Sheykhi, S.; Castellano, F. N. Controlling Thermally Activated Delayed Photoluminescence in CdSe Quantum Dots through Triplet Acceptor Surface Coverage. *J. Phys. Chem. Lett.* **2021**, *12* (15), 3718−3723.
(126) Li, Z. J.; Li, S.; Davis, A. H.; Hofman, E.; Leem, G.; Zheng, W. Enhanced Singlet Oxygen Generation by Hybrid Mn-Doped Nanocomposites for Selective Photo-Oxidation of Benzylic Alcohols. *Nano Res.* **2020**, *13* (6), 1668−1676.
(127) Lin, X.; Chen, Z.; Han, Y.; Nie, C.; Xia, P.; He, S.; Li, J.; Wu, K. ZnSe/ZnS Core/Shell Quantum Dots as Triplet Sensitizers toward Visible-to-Ultraviolet B Photon Upconversion. *ACS Energy Lett.* **2022**, *7* (3), 914−919.
(128) Xu, Z.; Huang, Z.; Jin, T.; Lian, T.; Tang, M. L. Mechanistic Understanding and Rational Design of Quantum Dot/Mediator Interfaces for Efficient Photon Upconversion. *Acc. Chem. Res.* **2021**, *54* (1), 70−80.
(129) Huang, Z.; Lee Tang, M. Semiconductor Nanocrystal Light Absorbers for Photon Upconversion. *J. Phys. Chem. Lett.* **2018**, *9* (21), 6198−6206.

https://doi.org/10.1021/acsomega.3c03962
ACS Omega 2023, 8, 34328−34353